Metodologías de simulación de sistemas y equipos térmicos. Flujos turbulentos y aplicaciones en energía termosolar de concentración.

III ENCUENTRO DE INGENIERÍA DE LA ENERGÍA DEL CAMPUS MARE NOSTRUM (CMN)

Universidad de Murcia (UM) y Universidad Politécnica de Cartagena (UPCT)

27 de Septiembre de 2016

Carlos-David Pérez-Segarra
Centro Tecnológico de Transferencia de Calor (CTTC)
Universitat Politècnica de Catalunya-BarcelonaTech (UPC)

Contents

Part A:
UPC-BarcelonaTech
and the CTTC

Universitat Politècnica de Catalunya-BarcelonaTech

- Campuses/Schools in BCN province
- Campus of International Excellence (Barcelona Knowledge Campus) (UPC&UB). Energy Campus.
- People: PDI (2968), PAS (1865)
- Research groups: 208
- Budget (2015): 310.5 M€
- Technology transfer (2014): 50.3 M€
- Students (33138) (27324 bachelor; 3063 master; 2378 doctorate, 2794 permanent formation)

- 57 double degrees with 62 universities
- Studies: Bachelor (63), Masters (62) (7 Erasmus Mundus; 21 in English), Doctorate programs (68)
- 4926 scholarships for bachelor and master students

* Academic course 2014/15

The Heat and Mass Transfer Technological Center

- Research Centre of the Technical University of Catalonia – Barcelona Tech (UPC)
- Located in Terrassa (North-West of Barcelona), Spain
- Personnel: 50 people working full time (8 professors, 12 researchers, 30 PhD students)
- More than 60 research projects with companies and within national and EU frameworks in the last 10 years; more than 100 papers in prestigious international journals in the last 10 years

Two main research lines

Basic line

Mathematical formulation, numerical resolution and experimental validation of heat and mass transfer phenomena.

- Natural and forced convection
- Turbulence simulation (RANS, LES, DNS)
- Combustion
- Two-phase flow (VOF, two fluid models)
- Solid-liquid phase change (PCM materials)
- Radiation (surface and participating media)
- Porous media
- Computational Fluid Dynamics and Heat Transfer (CFD&HT)
- Compressible effect and noise evaluation
- Computational Structure Dynamics (CSD) and Fluid Structure Interaction (FSI)
- Aerodynamics
- High performance computing: Numerical algorithms and solvers, parallel computing, etc.

Applied and TT line

Thermal and fluid dynamic optimization of thermal systems and equipment. Application of the acquired know-how from the basic studies

- Refrigeration (vapour compression cycles, absorption refrigeration, compressors, exp. devices, etc.)
- HVAC (ventilation, diff. contaminants in buildings,...)
- Active and passive solar systems (solar collectors using TIM, building facades with transp. layers, etc.)
- Concentrated Solar Power (CSP) (solar tower, storage tanks, etc.)
- Wind energy (blade design, thermal nacelle, wind farms, etc.)
- Heat exchangers (single – phase and two – phase, combustion heaters, etc.)
- Heat storage by liquids and using PCM
- Engine cooling and air conditioning in the automobile and the aeronautical fields
- Aerodynamics
- Bioengineering, etc.

Computational tools

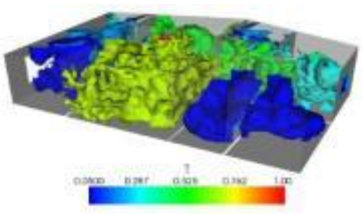

CFD&HT: Termofluids code

- 3D parallel unstructured code
- DNS, RANS and LES turbulence models
- Dynamic mesh methods for CSD and FSI
- Multi physics modelling (muti-phase, combustion, radiation, mass transfer, etc.)

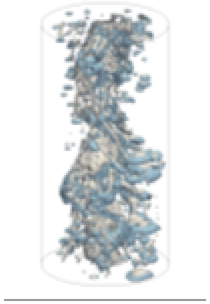

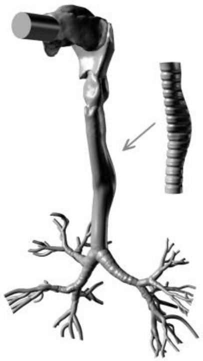

Object Oriented tools for thermal systems and equipment: NEST code

- Modular object-oriented buildings (rooms, walls, HAM+VOC; IAQ, active virtual control): NEST buildings
- Multiscale wind energy applications: NEST wind farms
- Multiscale approach solar tower receivers: NEST CSP
- Thermal Energy Storage Tanks: NEST STES & LTES
- Vapor Compression, absorption and adsorption refrigeration and systems: NEST cycle
- Condensers, evaporators and radiators: NEST HX
- Compressors in refrigeration field: NEST compressors

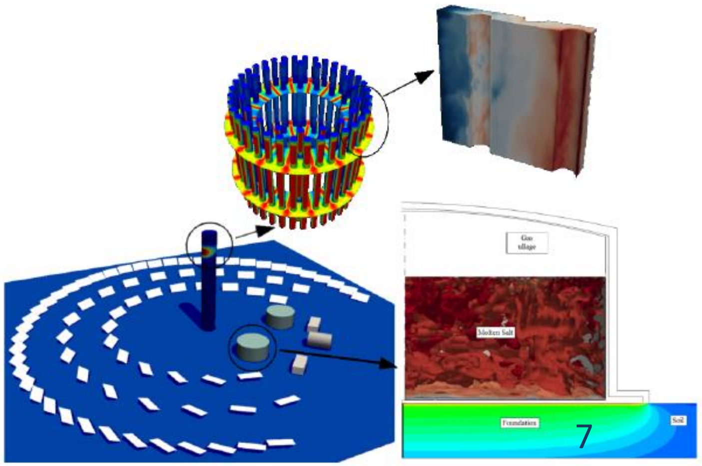

HPC facilities and parallelization capabilities

CTTC High Performance Cluster (HPC – JFF)

- Beowulf HPC-JFF cluster. Infiniband QDR 4X network interconnection between nodes with latencies of 1.07 μs with 40Gbits/s bandwidth
- More than 2300 processing cores
- The system of files allow unified capacities of several Petabytes highly scalable

TermoFluids CFD software as HPC platform

- More than 30 HPC R&D projects carried out with TF platform at the Spanish supercomputing network (RES)
- Three Tier0 research projects granted by PRACE with more that 30M core each
- Scalability tests up to 131K CPU-cores

~ 2 Petaflops for a single job (Mira ALCF)

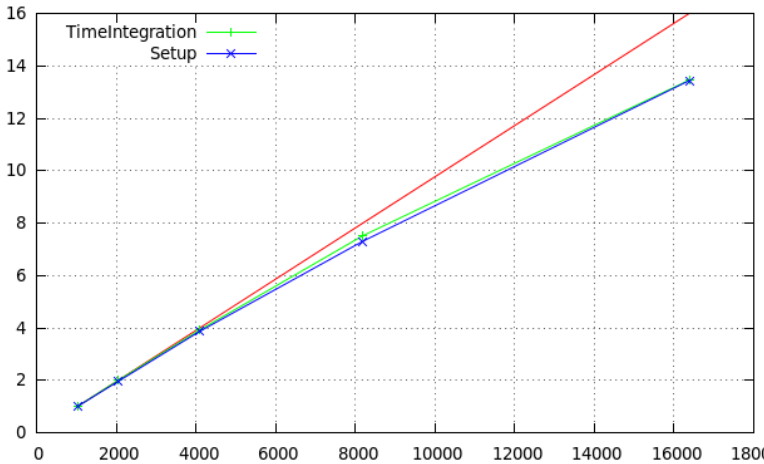

Parallel efficiency of above 80% for both the pre-processing and time-integration phases of the code (from 1024 up to **16384 CPU-cores** with 6000 cv/core, Argonne ALCF supercomputer)

Experimental facilities

- Vapor compression refrigerating systems (R600a, R134a, CO_2, etc.)
- Calorimeter compressor test
- Fin and tube heat exchangers test loop
- Climate chamber
- Motor bench
- Storage tanks
- Flat plate solar collectors
- Different types of ventilated façades
- Bioclimatic building
- Set-up for microchannel heat exchangers



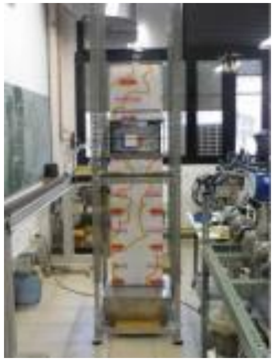
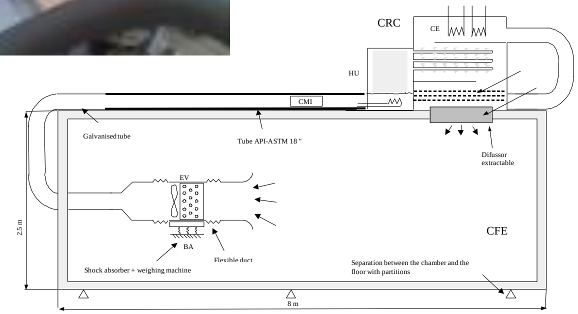





Part B: Turbulence

Vincent van Gogh

Leonardo da Vinci

Introduction to turbulence physics

- Turbulence is the usual state of motion of fluids except at low Reynolds numbers
- At high Reynolds numbers the non-linearity of the advection process leads to instabilities making the flow unsteady and 3D
- Turbulence contains a continuous spectrum of scales.

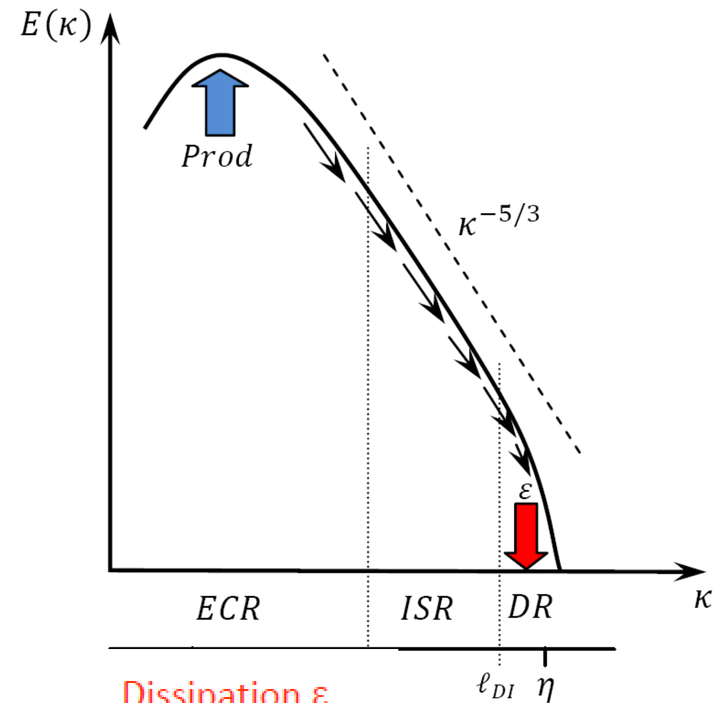

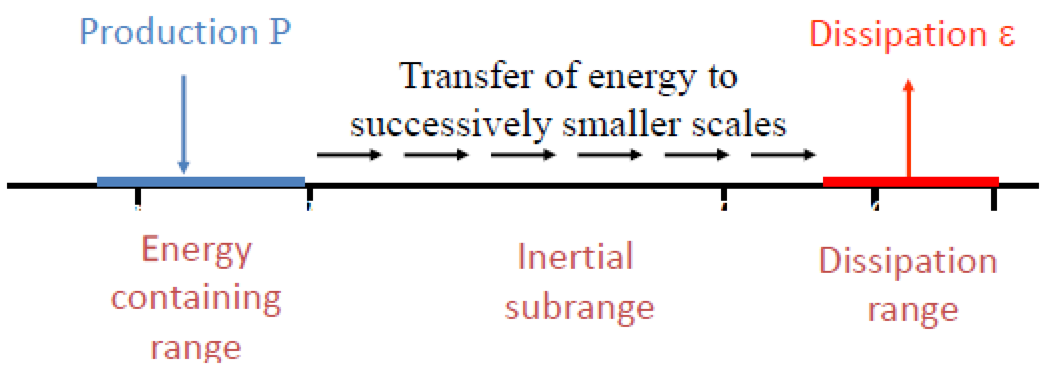

Introduction to turbulence physics

The inertial sub-range is general and "case" independent

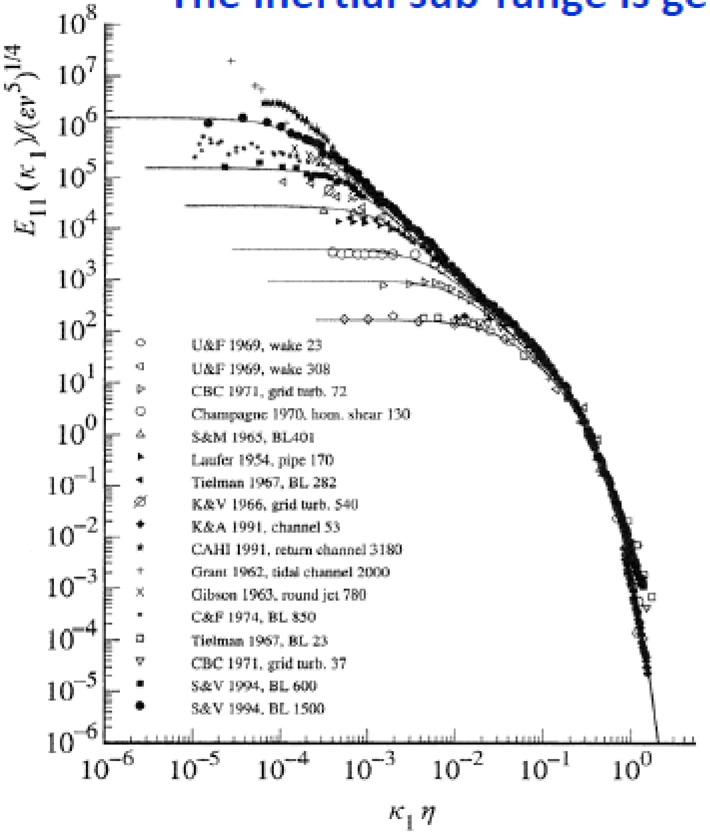

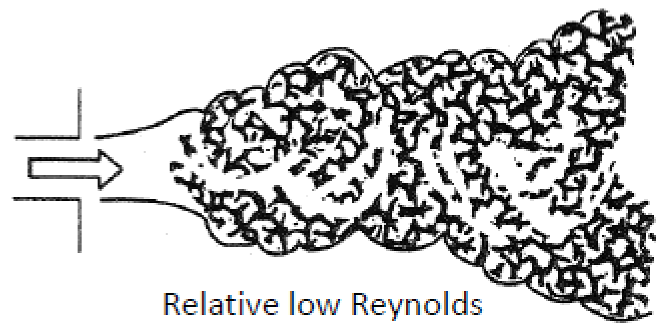

Relative low Reynolds number

Relative high Reynolds number

Sources: (left) S.B.Pope, Turbulent Flows, Cambridge University Press,; 2000; (right)H.Tennekes and J.L.Lumley, A first course in turbulence, The MIT Press, 19 72.

Introduction to turbulence physics

At the inertial sub-range the turbulence is homogeneous

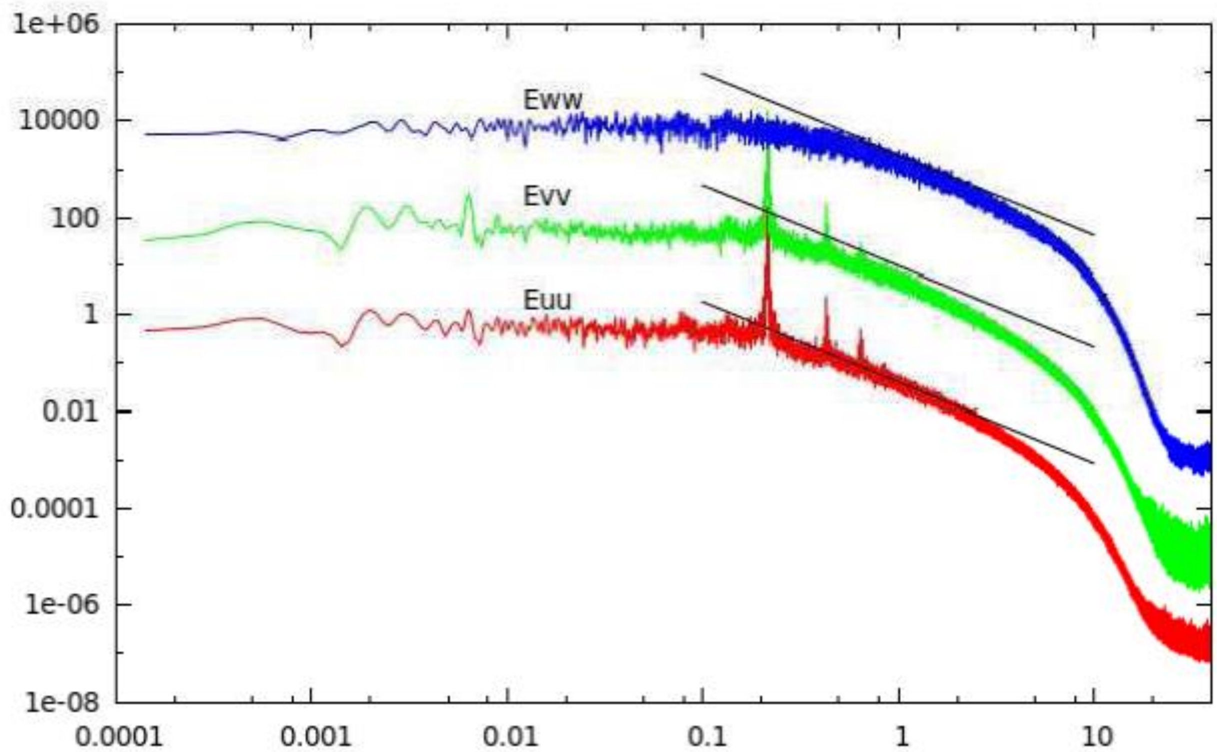

Introduction to turbulence physics

- Laminar and turbulent flows are governed by the same equations (continuum hypothesis is also suitable for turbulence)
- NS equations for incompressible Newtonian fluids

$$\nabla \cdot \boldsymbol{u} = 0$$

$$\frac{\partial \boldsymbol{u}}{\partial t} + (\boldsymbol{u} \cdot \nabla)\boldsymbol{u} = -\frac{1}{\rho}\nabla p + \nabla \cdot (2\nu \boldsymbol{S}) - \beta(T - T_o)\mathbf{g}$$

$$\frac{\partial T}{\partial t} + \boldsymbol{u} \cdot \nabla T = \frac{\lambda}{\rho c_p}\nabla^2 T$$

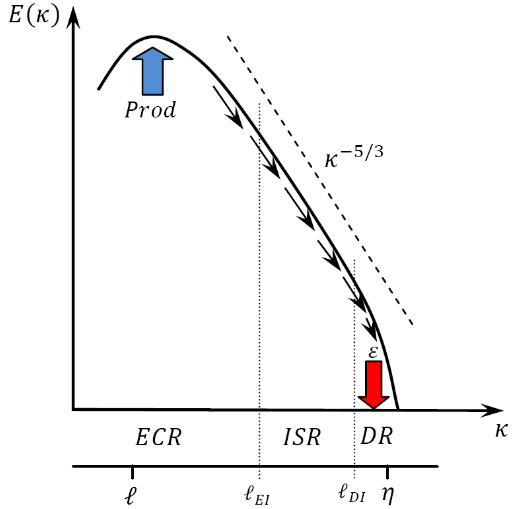

- DNS vs. LES vs. RANS …

Introduction to turbulence physics

DNS vs LES vs RANS

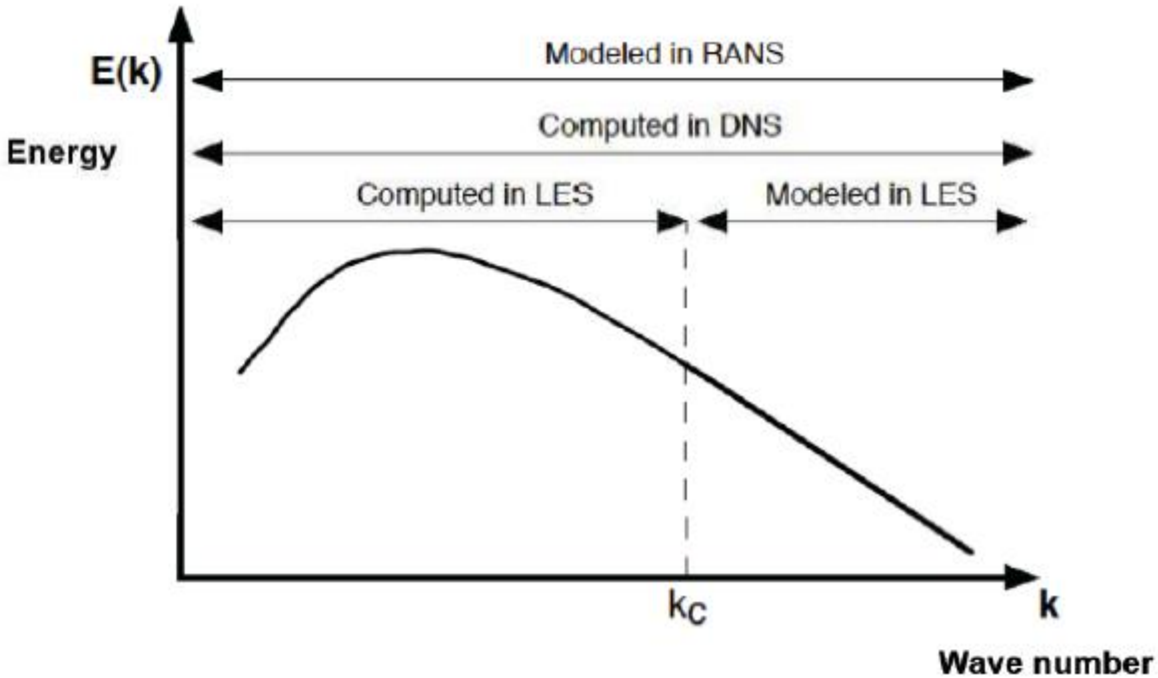

Introduction to turbulence physics

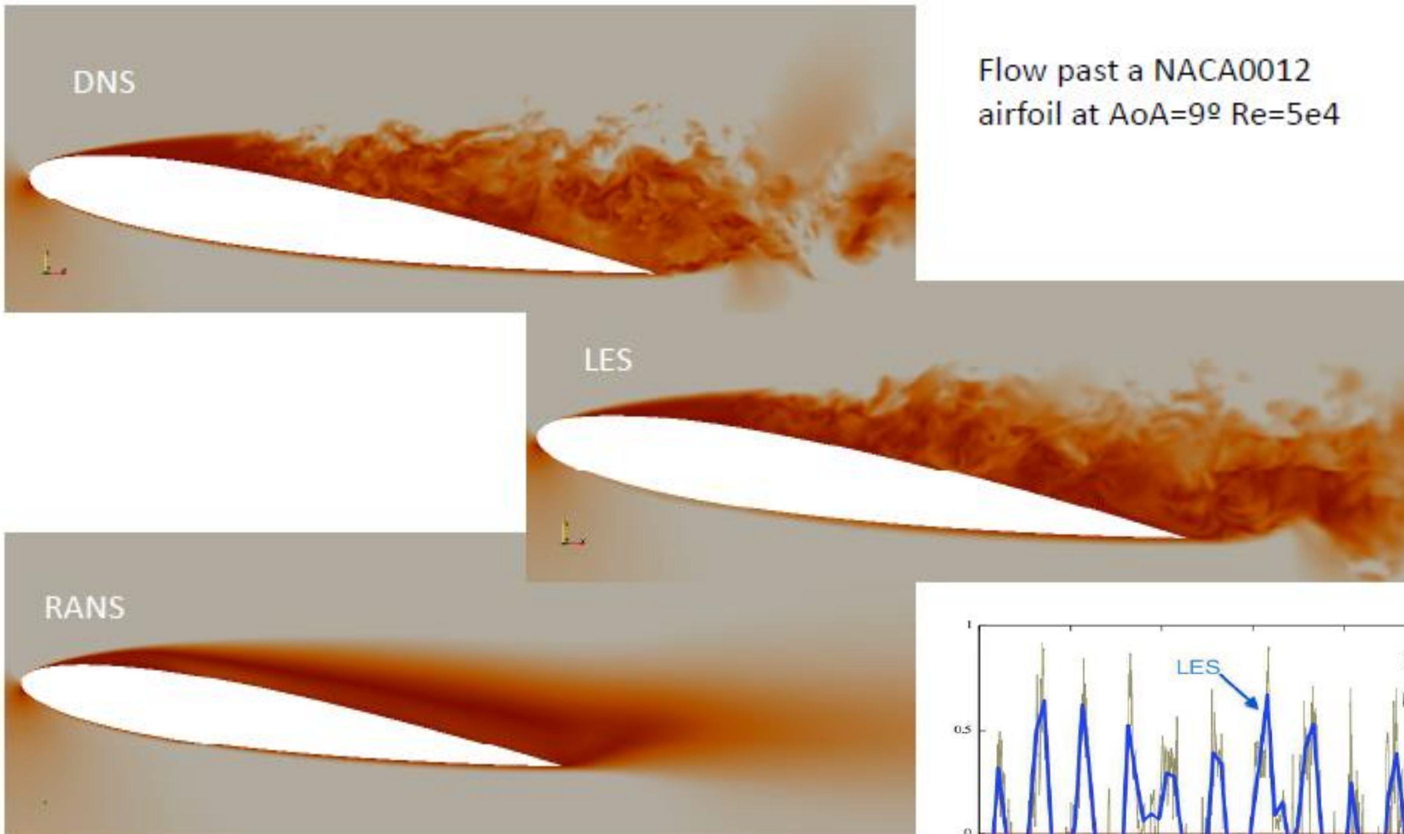

Flow past a NACA0012 airfoil at AoA=9º Re=5e4

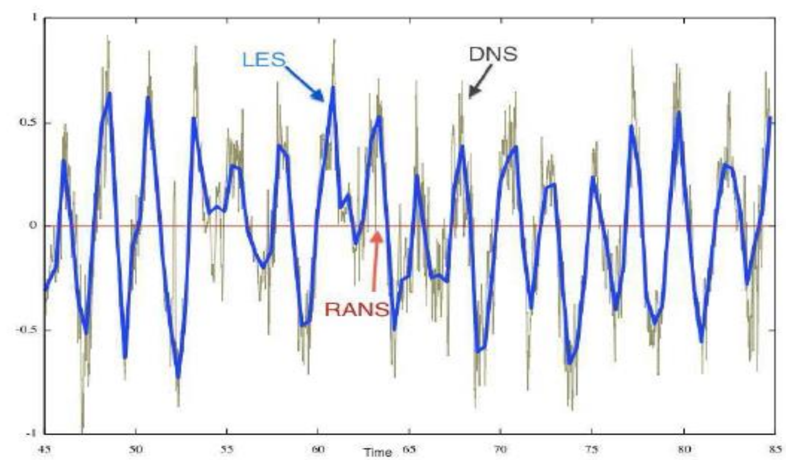

B1. Reynolds Averaged Navier-Stokes (RANS) Turbulence Models

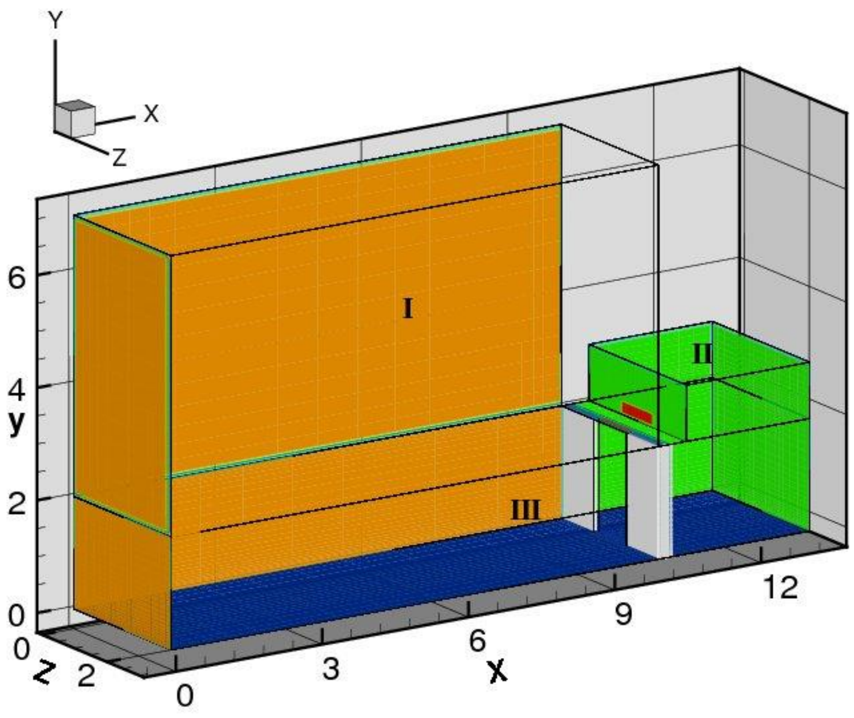

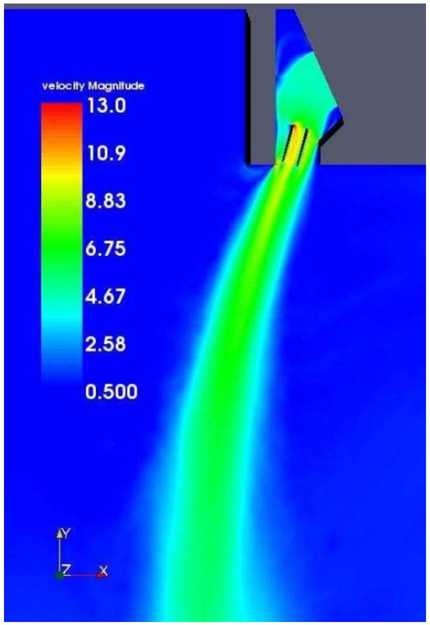

RANS – Mathematical formulation – Reynolds Averaged Navier-Stokes Equations (RANS)

- Instantaneous variables are expressed as:

$$\phi(\boldsymbol{x},t) = \bar{\phi}(\boldsymbol{x},t) + \phi'(\boldsymbol{x},t) = \frac{1}{\Delta t}\int_{t}^{t+\Delta t} \phi(\boldsymbol{x},t)dt + \phi'(\boldsymbol{x},t)$$

- RANS equations:

$$\nabla \cdot \overline{\boldsymbol{u}} = 0$$

$$\frac{\partial \overline{\boldsymbol{u}}}{\partial t} + (\overline{\boldsymbol{u}} \cdot \nabla)\overline{\boldsymbol{u}} = -\frac{1}{\rho}\nabla\bar{p} + \nabla \cdot \left(2\nu\overline{\boldsymbol{S}} - \overline{\boldsymbol{u}'\boldsymbol{u}'}\right) - \beta(\bar{T} - T_o)\boldsymbol{g}$$

$$\frac{\partial \bar{T}}{\partial t} + \overline{\boldsymbol{u}} \cdot \nabla\bar{T} = \nabla \cdot \left(\frac{\lambda}{\rho c_p}\nabla\bar{T} - \overline{\boldsymbol{u}'T'}\right)$$

RANS – Mathematical formulation – Hierarchy of turb. models

- Differential Reynolds Stress Models (**RSM**):

$$\frac{D\overline{u_i'u_j'}}{Dt} = d_{ij} + P_{ij} + G_{ij} + \phi_{ij} - \varepsilon_{ij}\,; \qquad \frac{D\overline{u_i'T'}}{Dt} = \cdots$$

- Algebraic (implicit or explicit) Reynolds Stress Models (**ARSM**):

$$f\left(\overline{u_i'u_j'}\right) = 0; \qquad \overline{u_i'T'} = -c_T\frac{k}{\varepsilon}\left(\overline{u_i'u_j'}\frac{\partial\bar{T}}{\partial x_j} + \xi\overline{u_k'T'}\frac{\partial\bar{u}_i}{\partial x_k} + \eta\beta\overline{T'T'}g_i\right)$$

- Linear eddy Viscosity Models (**LEVM** and **NLEVM**):

LEVM:
$$\overline{u_i'u_j'} - \frac{2}{3}k\delta_{ij} = -\nu_t\left(\frac{\partial\bar{u}_i}{\partial x_j} + \frac{\partial\bar{u}_j}{\partial x_i}\right); \qquad \overline{u_i'T'} = -\frac{\nu_t}{\sigma_T}\frac{\partial\bar{T}}{\partial x_i}$$

$$\nu_t = C_\mu f_\mu\frac{k^2}{\varepsilon} = C_\mu^* f_\mu^*\frac{k}{\omega}; \qquad \sigma_T = 0.9$$

NLEVM:
$$\frac{\overline{\boldsymbol{u}'\boldsymbol{u}'}}{k} - \frac{2}{3}\boldsymbol{I} = -2C_\mu f_\mu\boldsymbol{S} + \beta_1\left(\boldsymbol{S}\cdot\boldsymbol{S} - \frac{1}{3}[\boldsymbol{S}\cdot\boldsymbol{S}]\boldsymbol{I}\right) + \beta_2(\boldsymbol{W}\cdot\boldsymbol{S} - \boldsymbol{S}\cdot\boldsymbol{W})$$
$$+\beta_3\left(\boldsymbol{W}\cdot\boldsymbol{W} - \frac{1}{3}[\boldsymbol{W}\cdot\boldsymbol{W}]\boldsymbol{I}\right) - \gamma_1[\boldsymbol{S}\cdot\boldsymbol{S}]\boldsymbol{I} - \gamma_2[\boldsymbol{W}\cdot\boldsymbol{W}]\boldsymbol{S} - \gamma_3(\dots.) - \gamma_4(\dots.)$$

k and ε (or ω)?

RANS – Mathematical formulation – Turbulent transport equations

- Two extra transport equations are needed to obtain *k* and its dissipation rate (ε or ω)

$$\frac{\partial k}{\partial t} + \bar{\boldsymbol{u}} \cdot \nabla k = \nabla \cdot \left[\left(\nu + \frac{\nu_t}{\sigma_k} \right) \nabla k \right] + P_k + G_k - \varepsilon$$

$$\frac{\partial \tilde{\varepsilon}}{\partial t} + \bar{\boldsymbol{u}} \cdot \nabla \tilde{\varepsilon} = \nabla \cdot \left[\left(\nu + \frac{\nu_t}{\sigma_\varepsilon} \right) \nabla \tilde{\varepsilon} \right] + f_1 C_{\varepsilon 1} \frac{\tilde{\varepsilon}}{k} P_k + f_3 C_{\varepsilon 3} \frac{\tilde{\varepsilon}}{k} G_k - f_2 C_{\varepsilon 2} \frac{\tilde{\varepsilon}^2}{k} + E + Y_c$$

$$\frac{\partial \omega}{\partial t} + \bar{\boldsymbol{u}} \cdot \nabla \omega = \nabla \cdot \left[\left(\nu + \frac{\nu_t}{\sigma_\omega} \right) \nabla \omega \right] + f_{\omega 1} C_{\omega 1} \frac{\omega}{k} P_k + f_{\omega 2} C_{\omega 2} \frac{\omega}{k} G_k - \beta \omega^2$$

where,

$$\tilde{\varepsilon} = \varepsilon + D; \quad P_k = -\overline{\boldsymbol{u}'\boldsymbol{u}'} : \nabla \bar{\boldsymbol{u}}; \quad G_k = -\beta \boldsymbol{g} \cdot \left(-\frac{\mu_t}{\sigma_T} \nabla \bar{T} \right) \text{(SGDH)}; \quad G_k = -\beta \boldsymbol{g} \cdot \left(-\frac{3}{2} \frac{C_\mu f_\mu}{\sigma_T} \overline{\boldsymbol{u}'\boldsymbol{u}'} \cdot \nabla \bar{T} \right) (GGDH)$$

RANS – Mathematical formulation – Turbulent models tested

	k-ε		k-ω	
LEVM	**IL** **GPC**	Ince-Launder, 1989 Goldberg-Peroomian-Chakravarthy, 1998	**WX** **WXT** **WXCD** **PDH+D**	Wilcox, 1993 Wilcox, 1994 Wilcox, 1998 Peng, Davidson and Holmberg, 1999
NLEVM	**CLS**	Craft-Launder-Suga, 1996	**LAR** **AJL**	Larsson, 1997 Abe-Jang-Leschziner, 2003
EARSM	**AMGS**	Abid-Morrison-Gatski-Speziale, 1996	**ARG** **WJO**	Abid-Rumsey-Gatski, 1995 Wallin-Johanson, 2000

RANS – Examples

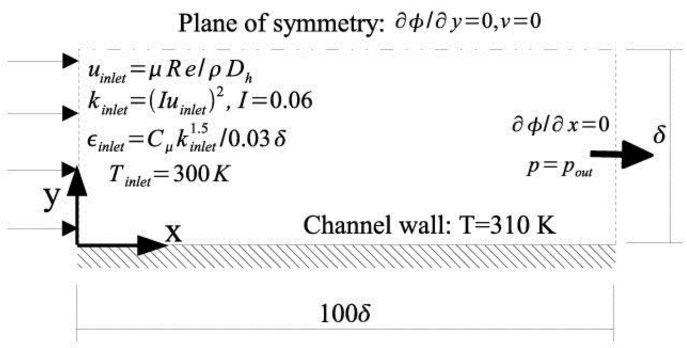

Plane channel flow

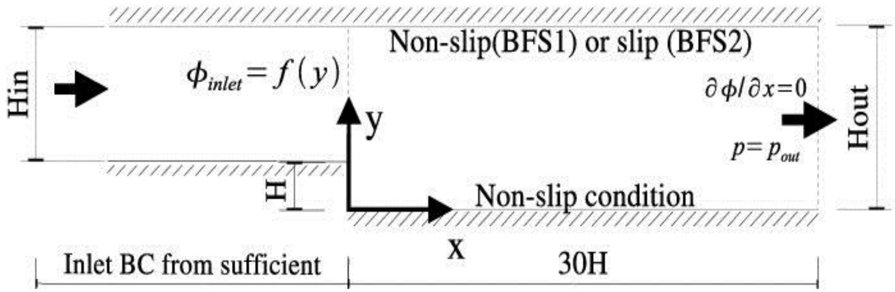

Backward facing step

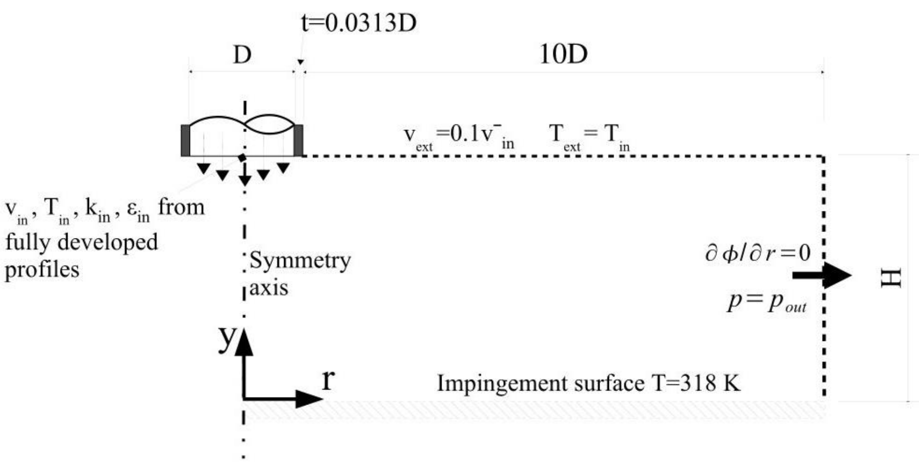

Plane and round jet

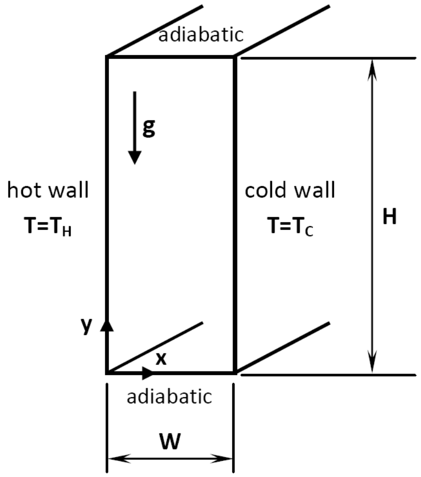

Differentially heated cavity

RANS – Examples – Plane channel flow

- Geometry, boundary conditions and computational domain

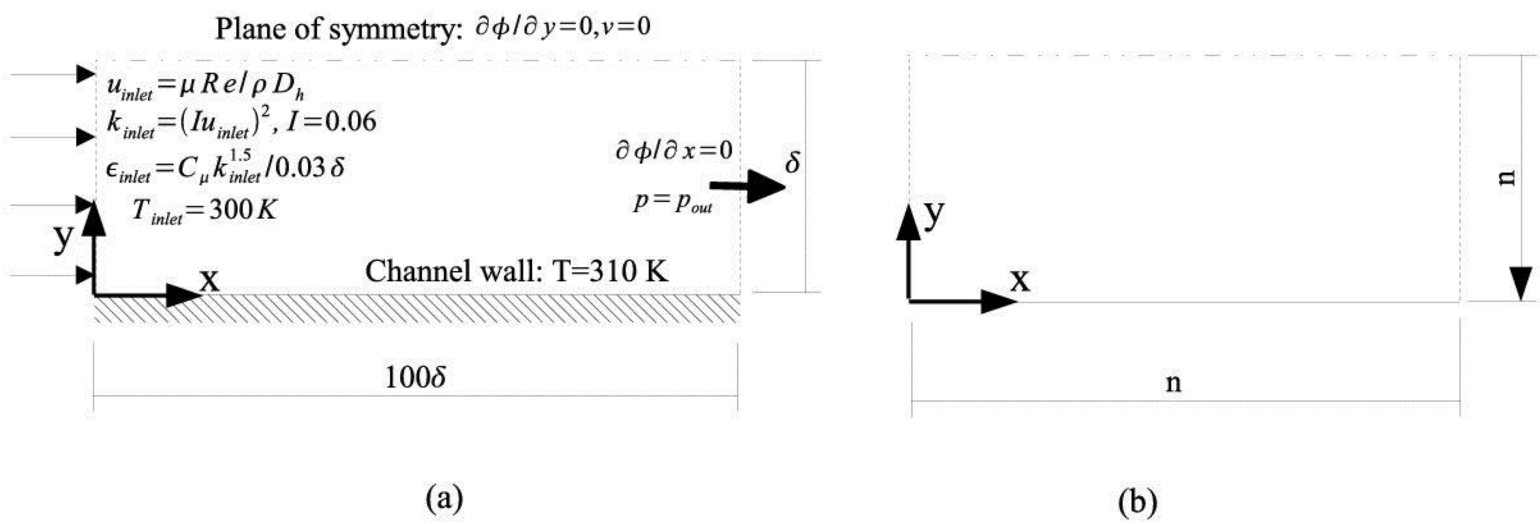

- Three cases: i) Re_t=180 (Re_{Dh}≈5640); ii) Re_t=395 (Re_{Dh}≈13800); iii) Re_t=590 (Re_{Dh}≈21700).
- DNS data by R.Moser et al. (Physics of Fluids 11:943-945, 1999).

RANS – Examples – Plane channel flow (Re$_\tau$=395, Re$_{2\delta}$≈13800)

- Turbulent kinetic energy and streamwise Reynolds stresses

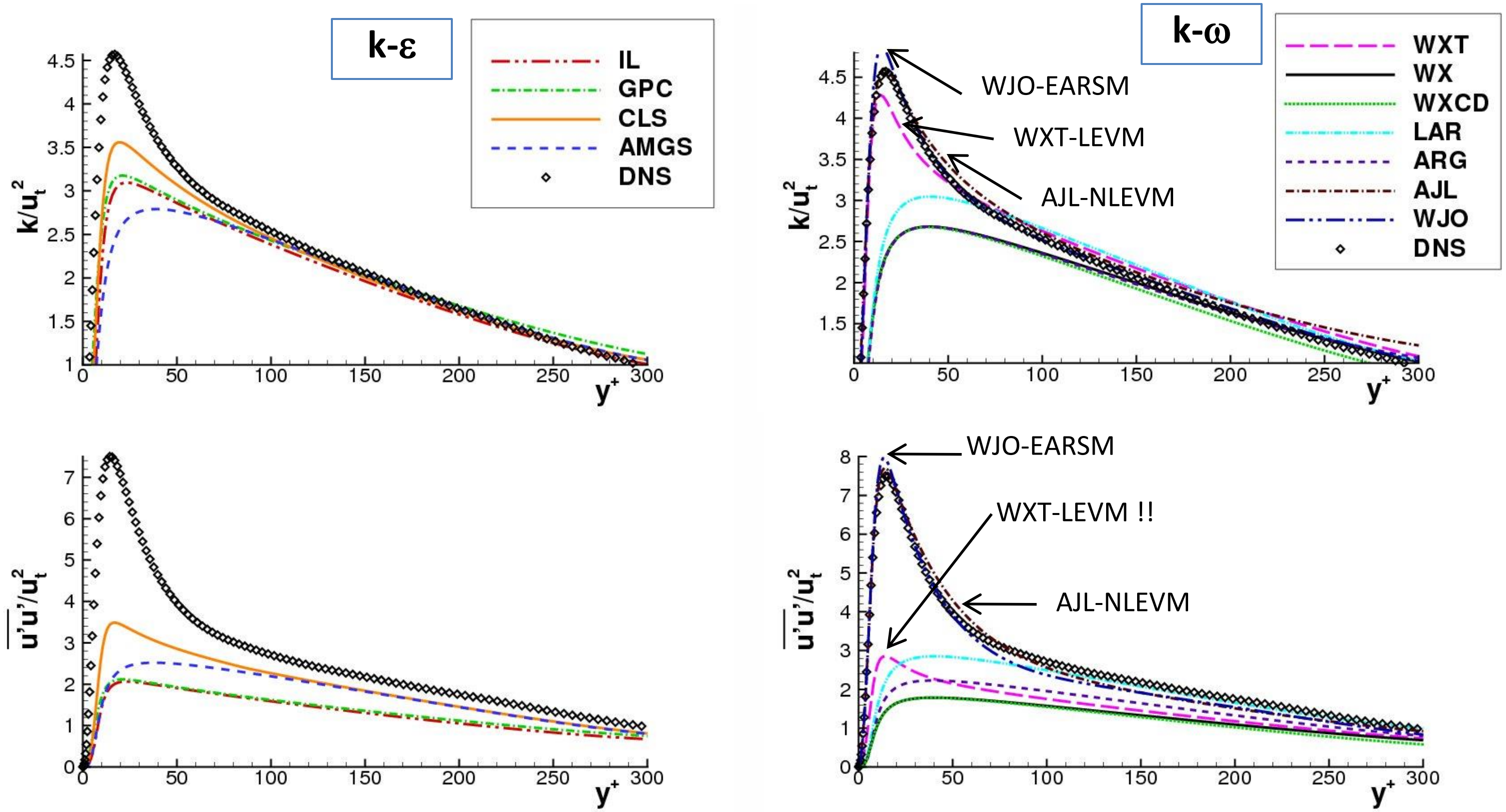

- k: good performance of AJL (kω-NLEVM), WJO (kω-EARSM), WXT (kω-LEVM)
- avrg(u'u'): well predicted by AJL (kω-NLEVM), WJO (kω-EARSM)
- In general, high-order k-ω models show better behaviour than k-ε models

RANS – Examples – Plane channel flow (Re_τ=395, $Re_{2\delta}\approx$13800)

- Normal Reynolds stresses in normal and spanwise directions

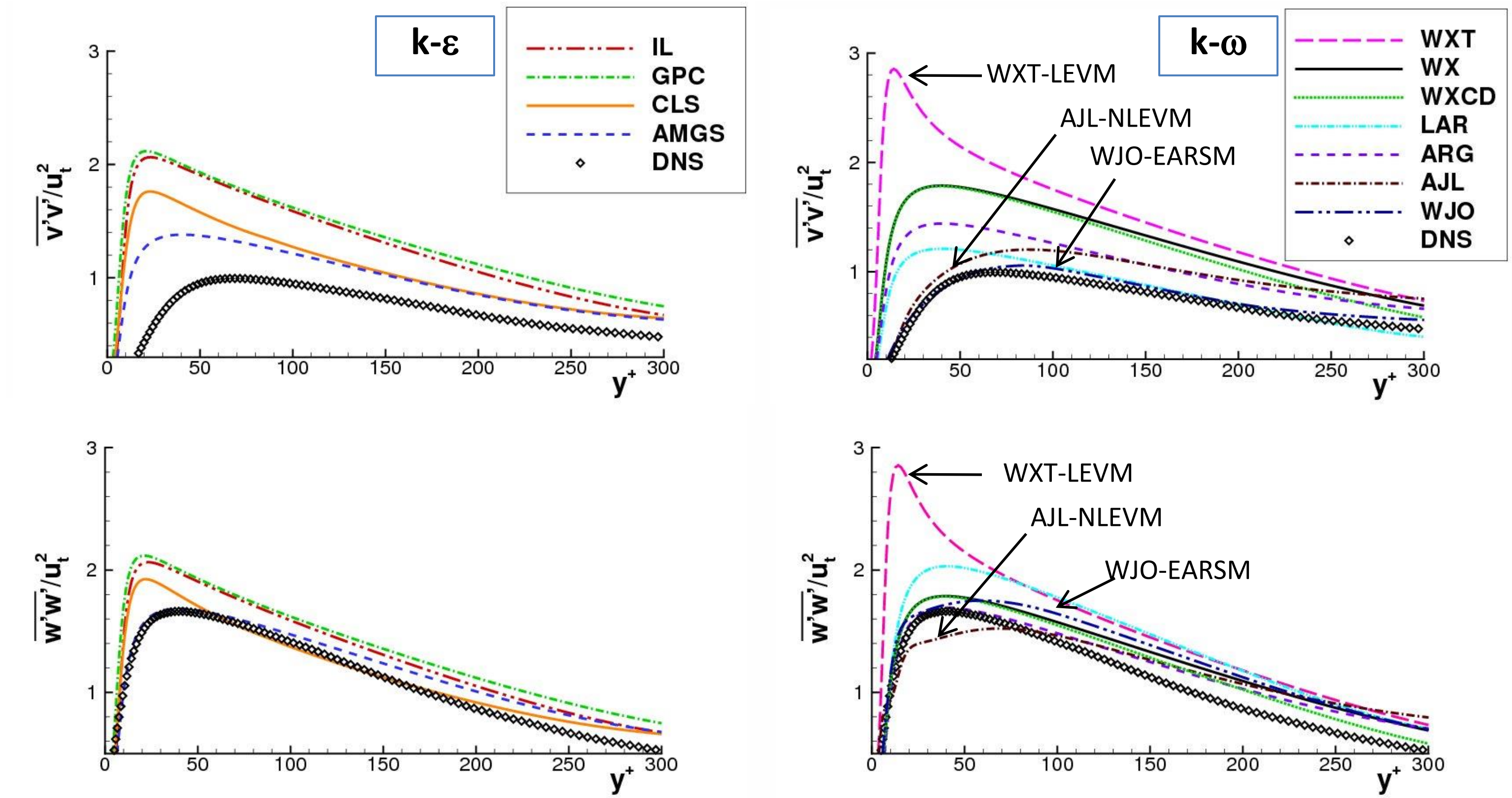

- Good prediction of k does not necessarily imply an adequate prediction of turbulent stresses
- EARSM and NLEVM perform better than LEVM

RANS – Examples – Backward facing step

- Geometry, boundary conditions and computational domain

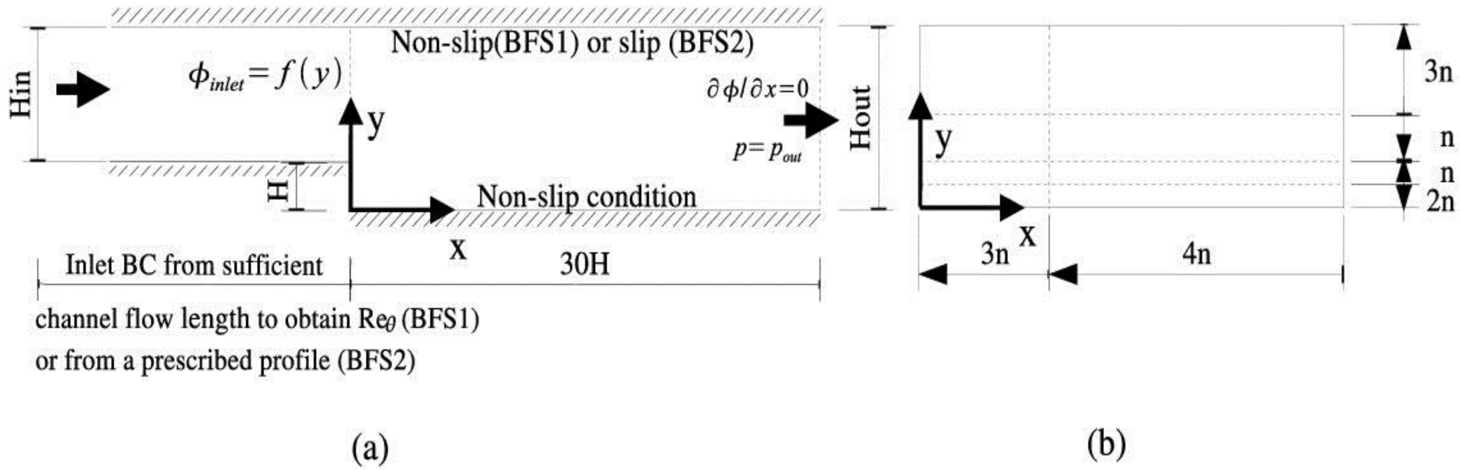

- Two configurations: BFS1 (Re_H=37500, ER=1.125), BFS2 (Re_H=28000, ER=1.25)
- Experimental data by Driver and Seegmiller (AIAA Journal, 23:163-171, 1985) for BFS1, and Vogel and Eaton (J. Heat Transfer, 107:922-929, 1985) for BFS2

RANS – Examples – Backward facing step (Re_H=37500, ER=1.125)

Reattachment point (X_r/H) and minimum skin-friction coefficient ($C_{f,min}$)

	Models	X_r/H	%	C_f min.x10^3	%
	Driver [63]	6.26±0.1	-	1.02	-
	IL	5.85	-6.55	1.612	58.04
	GPC	6.13	-2.08	1.405	37.74
	CLS	6.54	4.47	1.275	25.00
	AMGS	6.89	10.06	1.603	57.16
	WX	5.87	-6.23	1.244	21.96
	WXT	6.28	0.319	1.151	12.84
	WXCD	6.19	-1.12	1.248	22.35
	LAR	6.46	3.19	0.862	-15.49
EARSM	ARG	6.32	0.895	1.081	5.98
EARSM	WJO	6.55	4.63	0.978	-4.12
NLEVM	AJL	6.05	-3.35	0.967	-5.19

- In general, better behaviour of NLEVM/EARSM than LEVM (especially in C_f prediction)
- ARG, WJO and AJL give quite good results

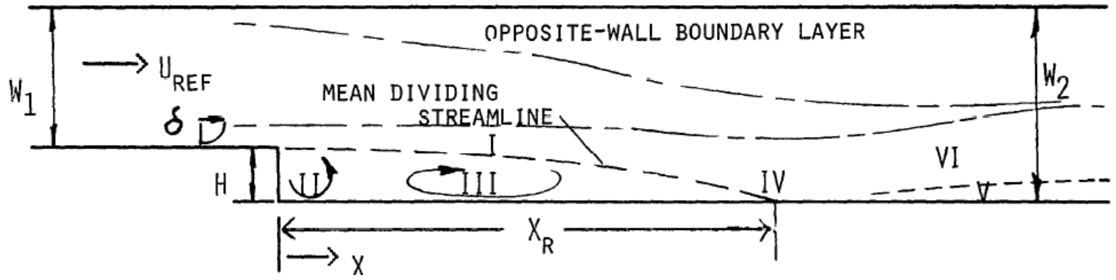

Figure from R.V.Westphal et al., NASA Contractor Report 3765, Jan 1984.

RANS – Examples – Backward facing step (Re_H=37500, ER=1.125)

- Skin friction coefficient

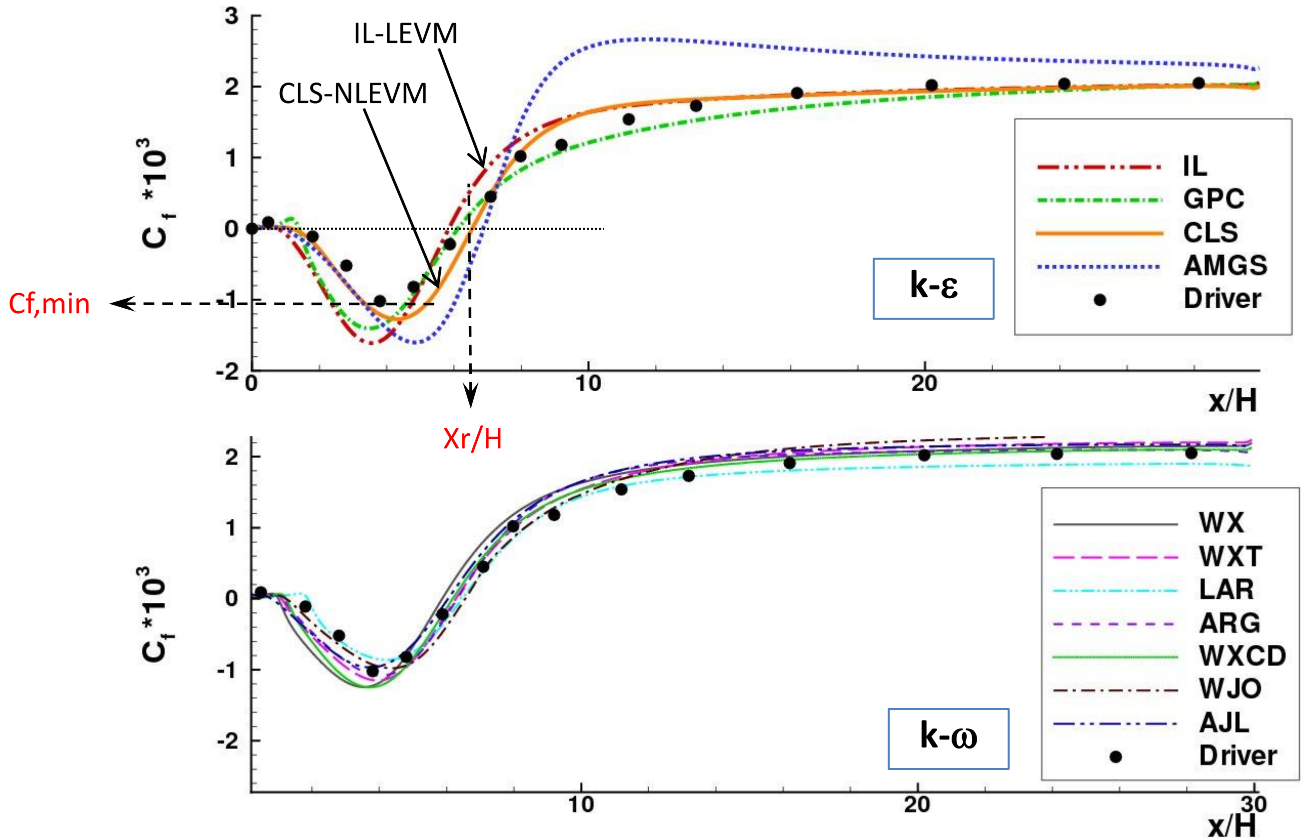

- k-ω models show less scattered and more accurate results than k-ε

RANS – Examples – Plane and round impinging jet

- Geometry, boundary conditions and computational domain

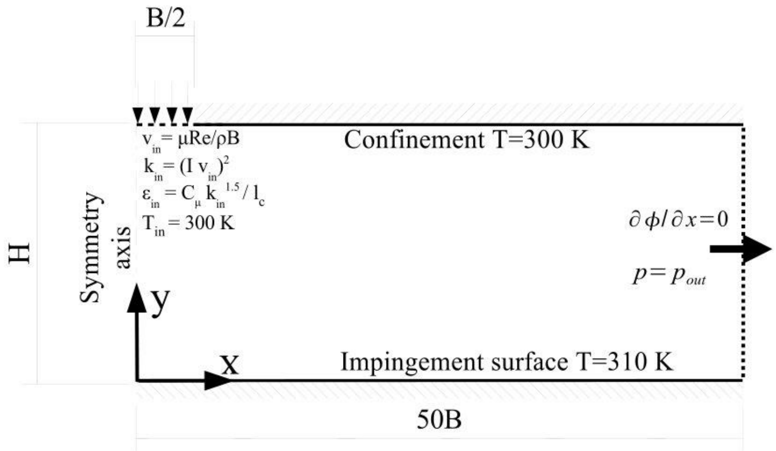

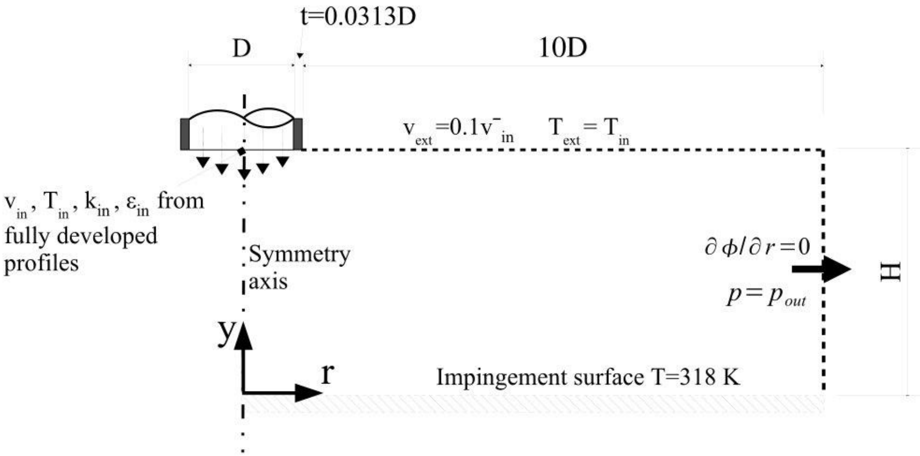

Plane impinging jet. Three cases: i) Re_B=10200, H/B=2.6; ii) Re_B=20000, H/B=4.0;iii) Re_B=30000, H/B=9.2. Pr=0.71.

Experimental data by Heiningen (PhD Thesis, 1982) (i); Ashforth-Frost (Exp. Therm. Fluid Sc., 14:60-67, 1997) (ii); Zhe and Modi (J. Fluid Eng., 123:112-120, 2001) (ii)&(iii).

Round impinging jet. Two cases: i) Re_D=23000, H/D=2; ii) Re_D=70000, H/D=6. Pr=0.71.

Experimental data by Baughn and Shimizu (J. Heat Transfer, 1989) (i)&(ii) - heat transfer; Cooper et al. (Int. J. Heat Mass Transfer, 1993) (i)&(ii) - velocities.

RANS – Examples – Plane impinging jet (Re_B=20000, H/B=4.0)

- Nusselt number at the impinging plate

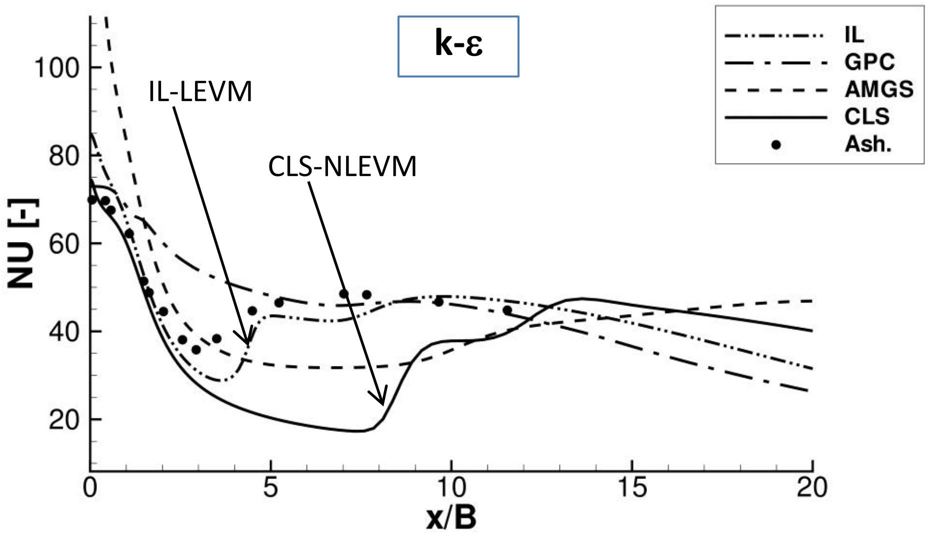

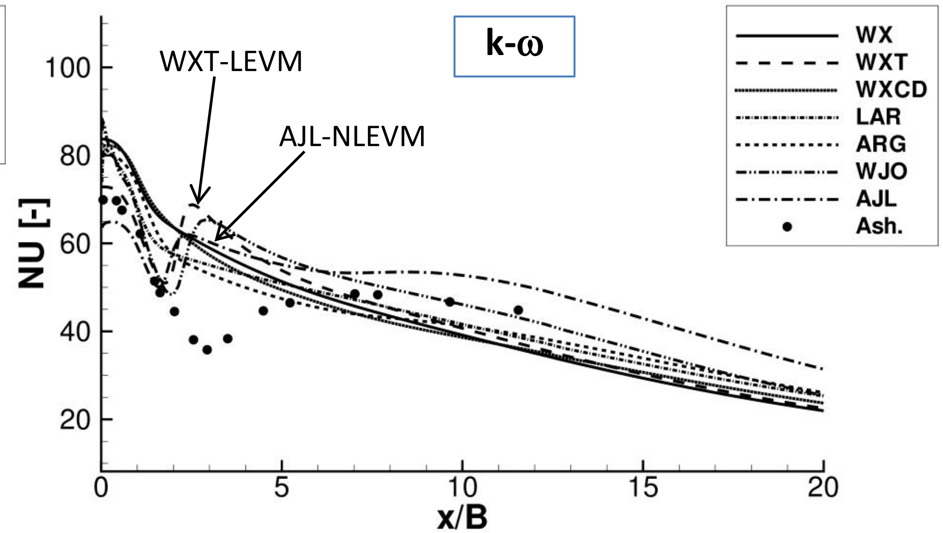

- Stagnation point: NLEVM and EARSM improve LEVM (see CLS vs. IL or LAR and ARG vs. WX). However, AMGS shows poor behaviour.
- Secondary maximum location: IL reasonably correct; CLS with delay; WXT, WJO and AJL too early

RANS – Examples – Plane impinging jet (Re_B=20000, H/B=4.0)

- x-velocity component of the mean velocity at two sections

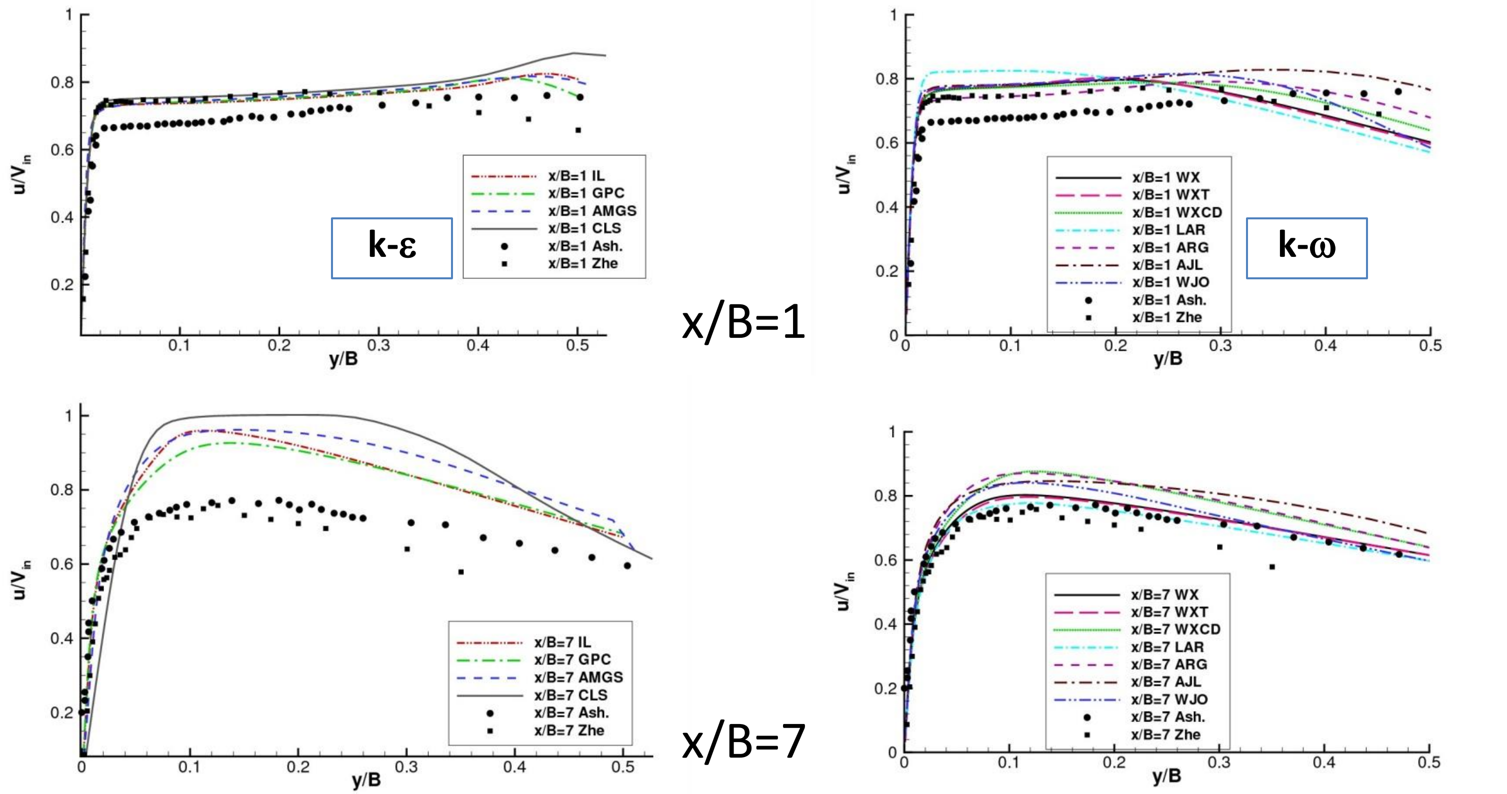

- At x/B=1, appropriate behaviour of all models respect to experimental data by Zhe and Modi.
- At x/B=7, all k-ε models have difficulties to reproduce experimental results.

RANS – Examples – Round impinging jet (Re_B=23000, H/D=2.0)

- Nusselt number at the impinging plate

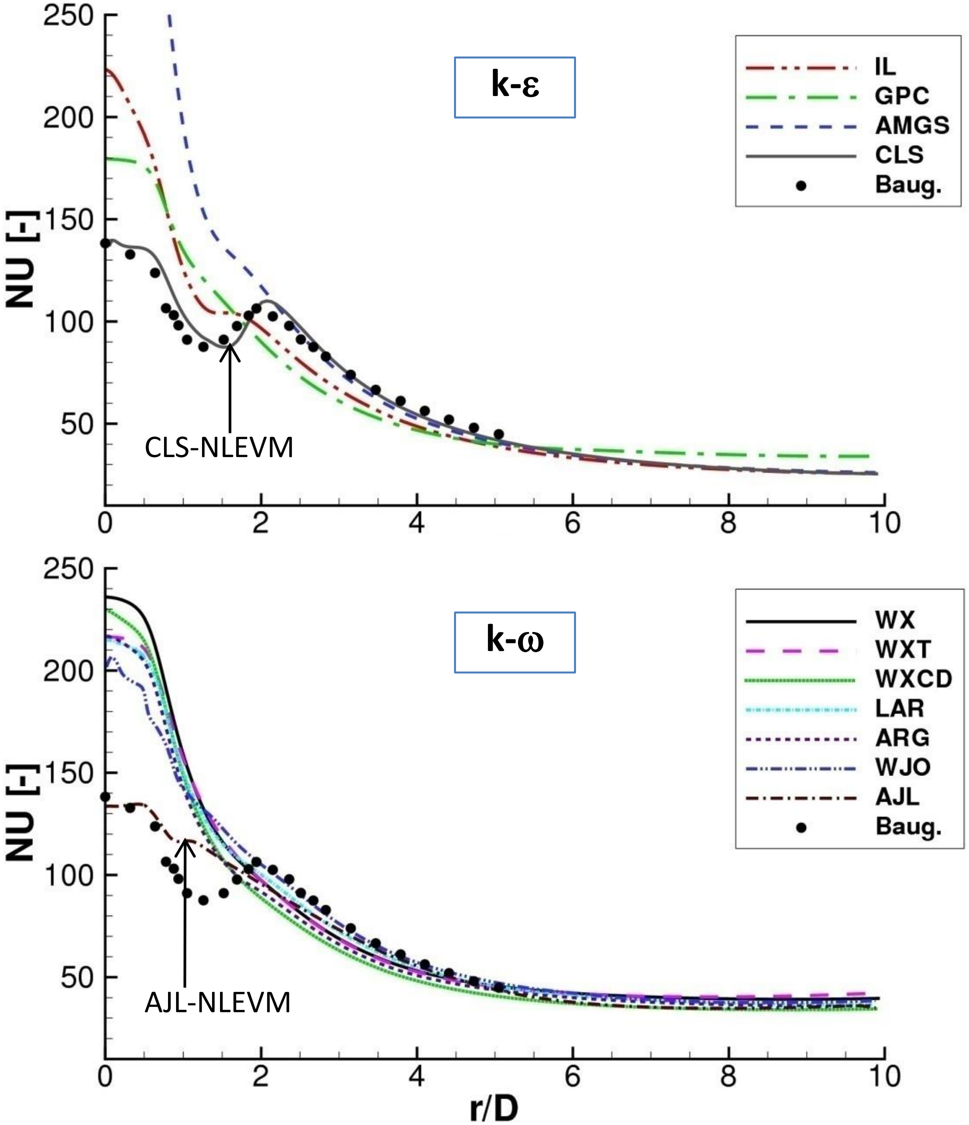

- CLS gives very good predictions.
- AJL improves LEVM predictions
- Different performance in plane and round impinging jet situations.

RANS – Examples – Round impinging jet (Re_B=23000, H/D=2.0)

- rms velocity in r-direction at two sections: r/D=0.5 and r/D=1

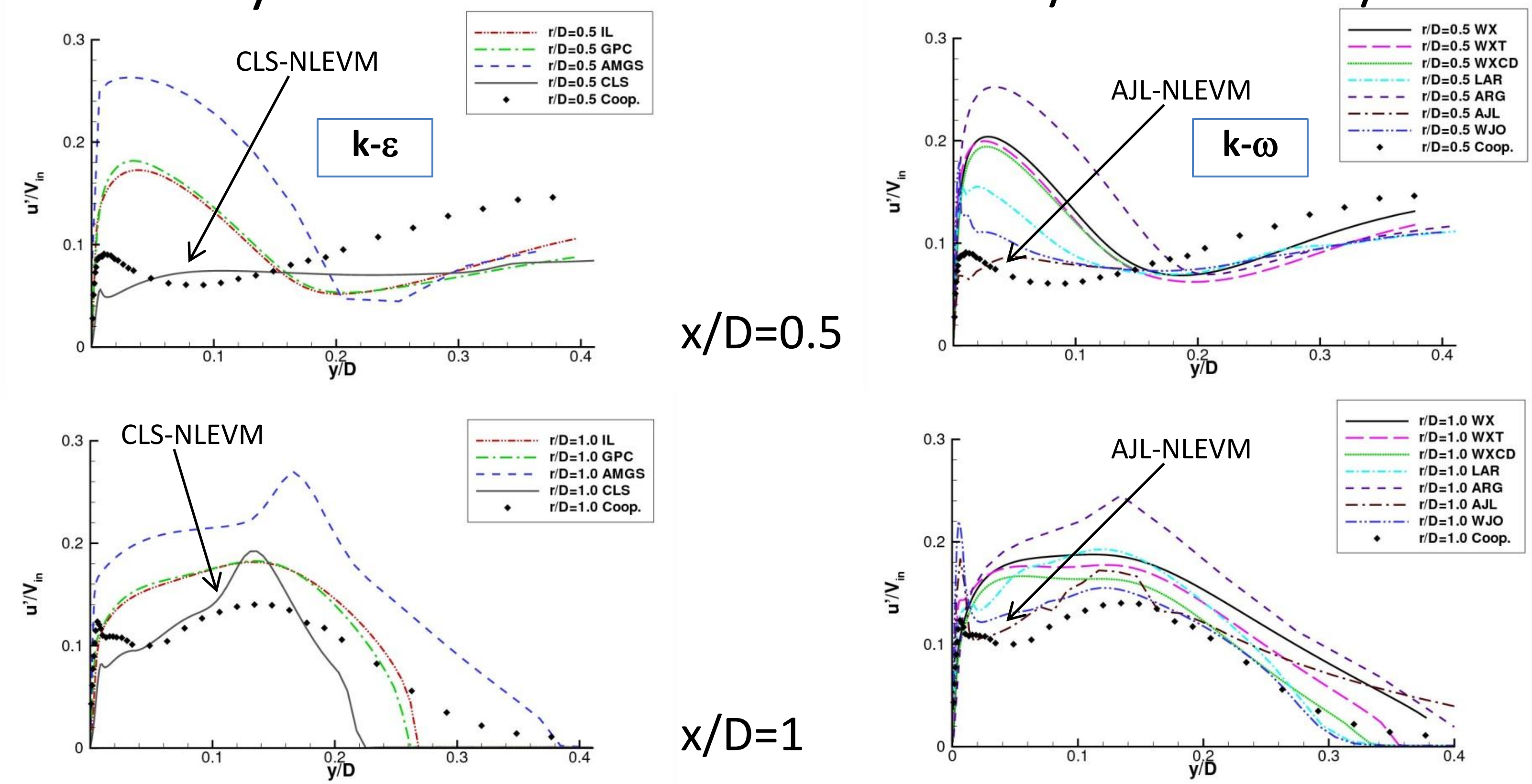

- LEVM overpredict fluctuating velocity near the stagnation point
- LEVM give high turbulence level producing too much jet spreading
- Using CLS and AJL considerable improvements are obtained.

RANS – Examples – Differentially heated cavity

- Geometry and boundary conditions

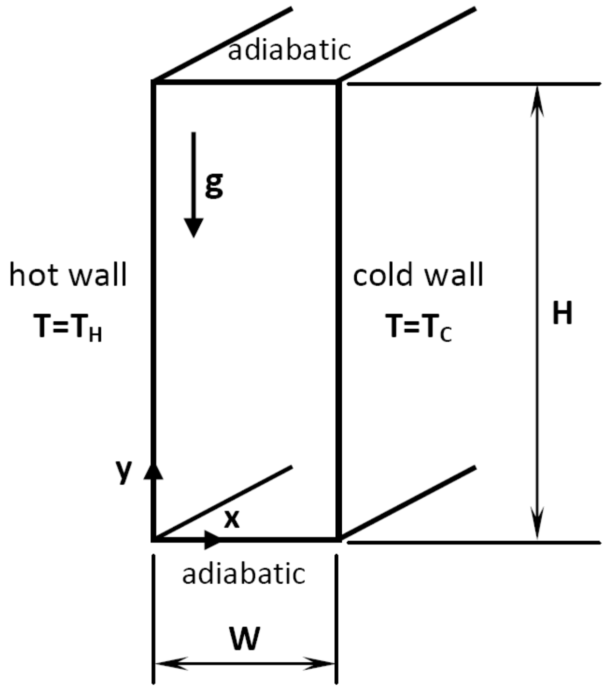

- Four cases tested: i) *A=H/W=30* (tall cavity), $Ra_H=2.43x10^{10}$, *Pr=0.71*; ii) *A= 5*, $Ra_H=5x10^{10}$, *Pr=0.71; iii) A=4*, $Ra_H=1x10^{10}$ and $Ra_H=1x10^{11}$, *Pr=0.71.*
- Experiments by Daffa'alla and Betts for *A=30* (Exp. Heat Transfer, 1996); Cheesewright et al for *A=5* (Procc., 1986); and DNS results *A=4* (CTTC results).

RANS – Examples – DHC (A=4, $Ra_H=10^{10}$)

- Nusselt number distribution at the hot wall

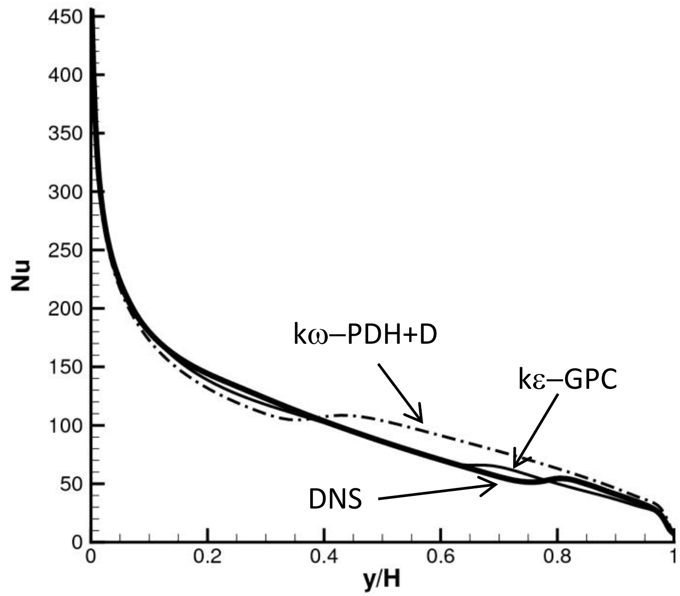

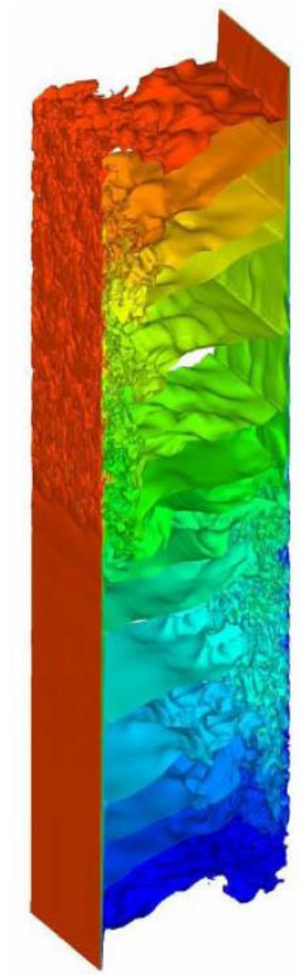

- A=30, all tested models (IL, GPC, WX, WXT, PDH+D) give reasonable accurtae results (specially IL)
- A=5 and A=4, IL delays transition when the grid is refined (eventually the flow becomes fully laminar). WX and WXT do not present this problem but they give poor results.
- A=5 and A=4, IL delays transition when the grid is refined (eventually the flow becomes fully laminar). WX and WXT do not present this problem but they give poor results.

RANS – Examples – Differentially heated cavity (A=4, $Ra_H=10^{10}$)

Dimensionless temperature and vertical velocity profiles at y/H=0.5

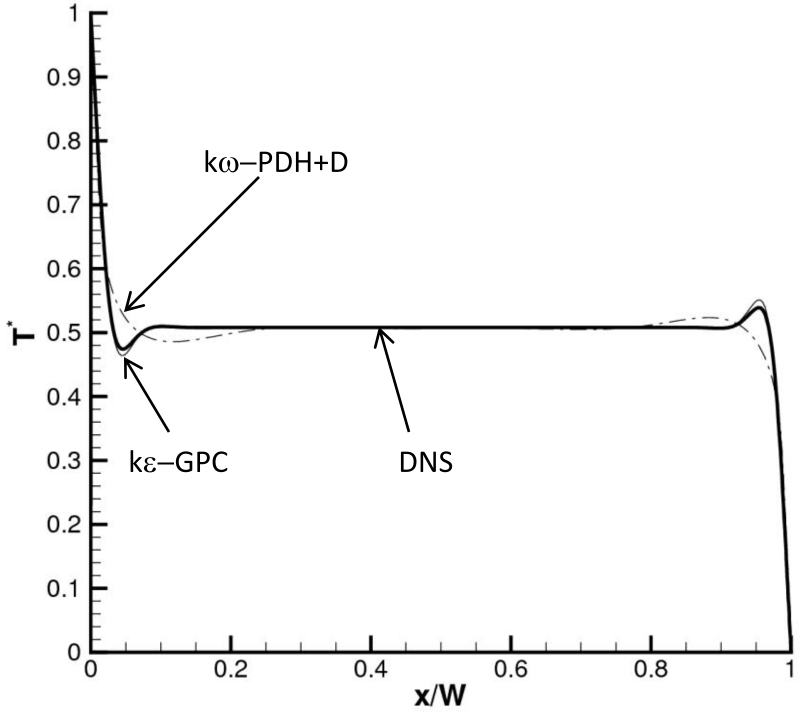

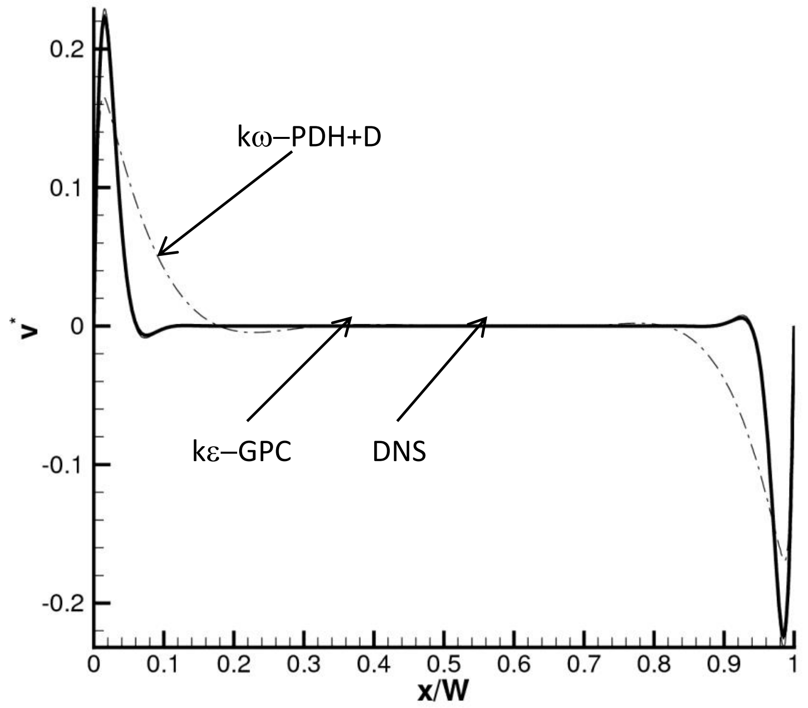

- GPC: accurate velocity and temperature profiles. PDH+D results are affected by the predicted early transition.
- Second-order statistics are not very well predicted.

B2. Direct Numerical Simulation (DNS) and Large Eddy Simulation (LES)

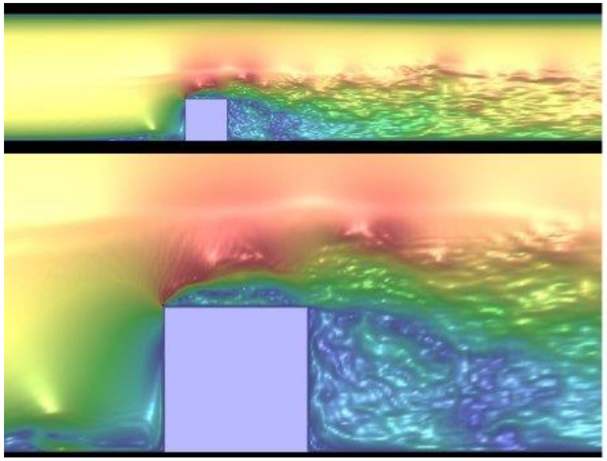

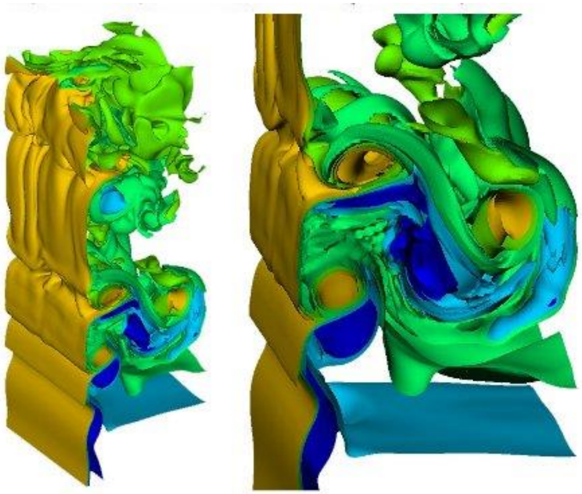

DNS- Direct Numerical Simulation

- Finite volume discretization of the continuity, Navier-Stokes and energy equations for all of the *N*-CVs the domain is discretized using arbitrary collocated meshes

$$M_c \boldsymbol{u_c} = 0$$

$$\boldsymbol{\Omega_c} \frac{\partial \boldsymbol{u_c}}{\partial t} + C_c(\boldsymbol{u_c})\boldsymbol{u_c} = \nu D_c \boldsymbol{u_c} - \rho^{-1} \boldsymbol{\Omega_c} G_c \boldsymbol{p_c} + \boldsymbol{\Omega_c} \boldsymbol{f_c}$$

$$\boldsymbol{\Omega_c} \frac{\partial \boldsymbol{T_c}}{\partial t} + C_c(\boldsymbol{u_c})\boldsymbol{T_c} = \lambda \rho^{-1} c_p^{-1} D_c \boldsymbol{T_c}$$

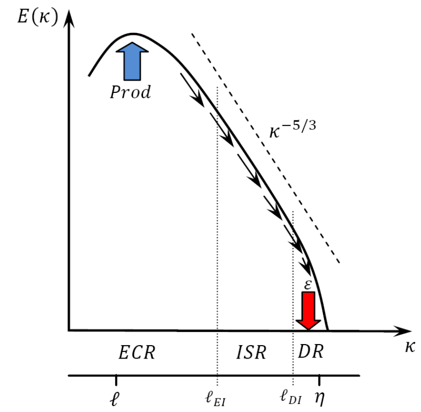

where,

$$\boldsymbol{u_c^*} = \{v_{x1}, v_{x2}, \dots, v_{xN}, v_{y1}, v_{y2}, \dots, v_{yN}, v_{z1}, v_{z2}, \dots, v_{zN}\}; \quad \boldsymbol{p_c^*} = \{p_1, p_2, \dots, p_N\}; \quad \boldsymbol{T_c^*} = \{T_1, T_2, \dots, T_N\}$$

- Direct Numerical Simulation (DNS) solves all relevant scales in turbulent flow. There are no model approximations.
- DNS approach: *5xN* equations with *5xN* unknowns ($\boldsymbol{u_c}$, $\boldsymbol{p_c}$, $\boldsymbol{T_c}$) must be solved at each Δt
- DNS demands accurate numerical schemes (guided by theory) and parallelization techniques.

DNS – Spatial discretization. Symmetry-preserving discretization

- Evolution equation of global kinetic energy (no body forces):

$$\frac{d}{dt}\|\boldsymbol{u_c}\|^2 = \frac{d\boldsymbol{u_c^*}\boldsymbol{\Omega}_c\boldsymbol{u_c}}{dt} = -\boldsymbol{u_c^*}\big(C_c(\boldsymbol{u_c}) + C_c^*(\boldsymbol{u_c})\big)\boldsymbol{u_c} - \nu\boldsymbol{u_c^*}(D_c + D_c^*)\boldsymbol{u_c} - \rho^{-1}\boldsymbol{u_c^*}\boldsymbol{\Omega}_c G_c\boldsymbol{p_c} - \rho^{-1}\boldsymbol{p_c^*}G_c^*\boldsymbol{\Omega}_c^*\boldsymbol{u_c}$$

- Our unstructured spatial discretization schemes are conservative, i.e. they preserve the kinetic energy equation. Main properties
  - Convective operator is skew symmetric, $C_c(\boldsymbol{u_c})=-C_c^*(\boldsymbol{u_c})$
  - Transpose of the discrete gradient operator is minus the discrete divergence operator, $(\Omega_c G_c)^*=-M_c$
  - Diffusion is a symmetric and positive definite operator, $\boldsymbol{u_c}^* (D_c+D_c^*)\, \boldsymbol{u_c} \geq 0$

DNS – The discretization is relevant!

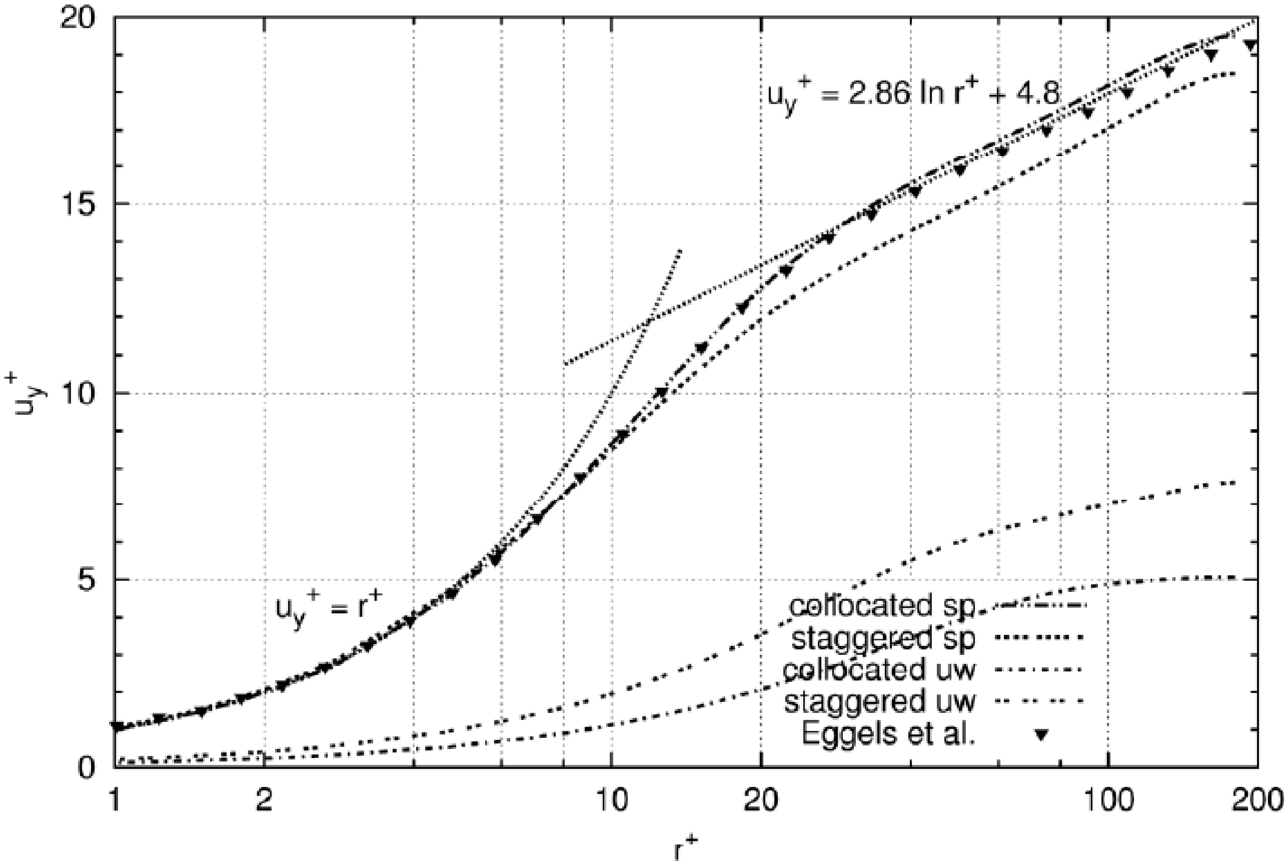

- Pipe flow at Re=5300
- Mesh size: 3M CV
- Unstructured momentum schemes: collocated 2nd order vs. staggered 1st order
- Convective schemes: energy conserving vs. upwind based
- Your NS discretization is going to change the "turbulent behaviour" of your model!

DNS – Numerical algorithm

- Integration algorithm: explicit fractional step projection method:
  1. At each instant, predicted velocity are firstly calculated, $\mathbf{u}_c^p$
  2. Evaluation of the Poisson equation for pressure, $\mathbf{p}_c^{n+1}$
  3. Then, velocities are updated, $\mathbf{u}_c^{n+1}$
  4. Finally, temperatures are explicitly evaluated, $\mathbf{T}_c^{n+1}$

- Parallelization: domain decomposition strategy + MPI
- Poisson solver:
  - Fully 3D flows: iterative Krylov methods (CG).
  - When flows with one periodic direction (z-direction in Cartesian coordinates or the θ-direction in axysymmetric flows): i) Fourier diagonalization to reduce the 3D equation to a family of independent 2D equations; ii) the 2D systems are solved by a Direct Schur decomposition method

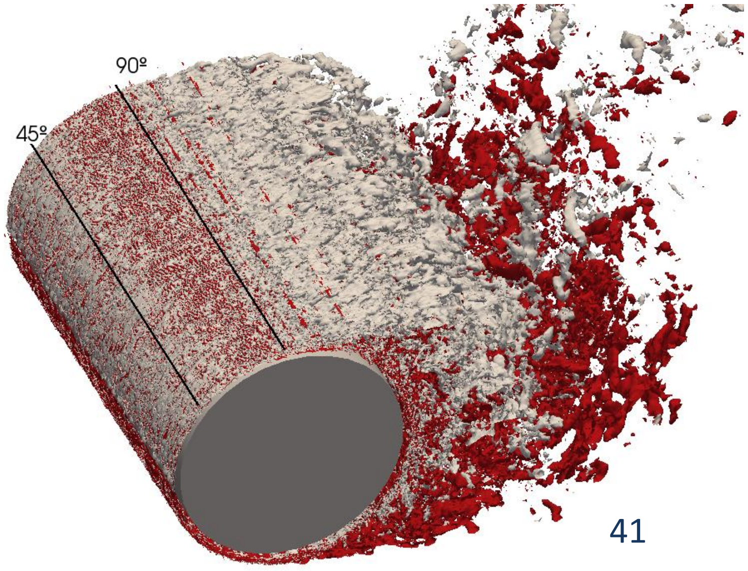

LES/RGM – Large Eddy Simulation

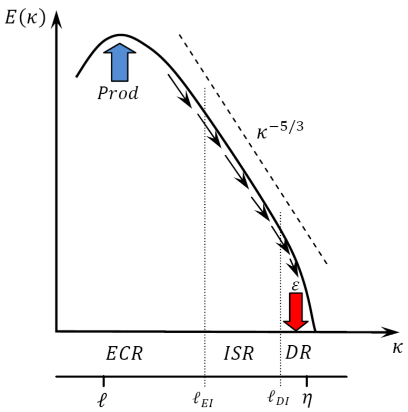

- The full energy spectrum can not be computed in most applications. A dynamically less complex math.formulation is needed.
- In **LES**, large scales are calculated while the effects of the smallest-scale motions are modelled. Three main steps:
  - Filtering operation: $\bar{\phi}(\boldsymbol{r},t) = \int_{\Omega} G(\boldsymbol{r}-\boldsymbol{\xi},\boldsymbol{\varepsilon})\phi(\boldsymbol{\xi},t)d\boldsymbol{\xi}$
  - Equations for the evolution of the filtered velocity field:

$$\boldsymbol{\Omega_c}\frac{\partial \bar{\boldsymbol{u}}_c}{\partial t} + C_c(\bar{\boldsymbol{u}}_c)\bar{\boldsymbol{u}}_c - \nu D_c\bar{\boldsymbol{u}}_c + \rho^{-1}\boldsymbol{\Omega_c}G_c\bar{\boldsymbol{p}}_c - \boldsymbol{\Omega_c}\bar{\boldsymbol{f}}_c = C_c(\bar{\boldsymbol{u}}_c)\bar{\boldsymbol{u}}_c - \overline{C_c(\boldsymbol{u}_c)\boldsymbol{u}_c} = -\mathcal{M}_c\boldsymbol{\mathcal{T}_c}$$

  - Modelling the SGS stress tensor. Simplest closure: $\boldsymbol{\mathcal{T}_c} \approx -2\nu_{sgs}\bar{\boldsymbol{S}}_c + (\boldsymbol{\mathcal{T}_c}:\boldsymbol{I})\boldsymbol{I}/3$
- LES models considered in this work:
  - Dynamic Smagorinsky LES Model (**Dynamic**)
  - Wall-Adapting Local Eddy-viscosity Model (**WALE**)
  - Variational Multiscale Method (**VMS**)
  - Verstappen Subgtid-Scale Model (**QR**)
- They allow near-wall analysis; wall-distance free; they drive to DNS when the mesh is refined enough.

DNS/LES/RGM – Backward Facing Step (Re_H=5100, ER=1.20)

- Horizontal velocity profiles at different sections (x/H=0.5, x/H=2.5, x/H=7.5)

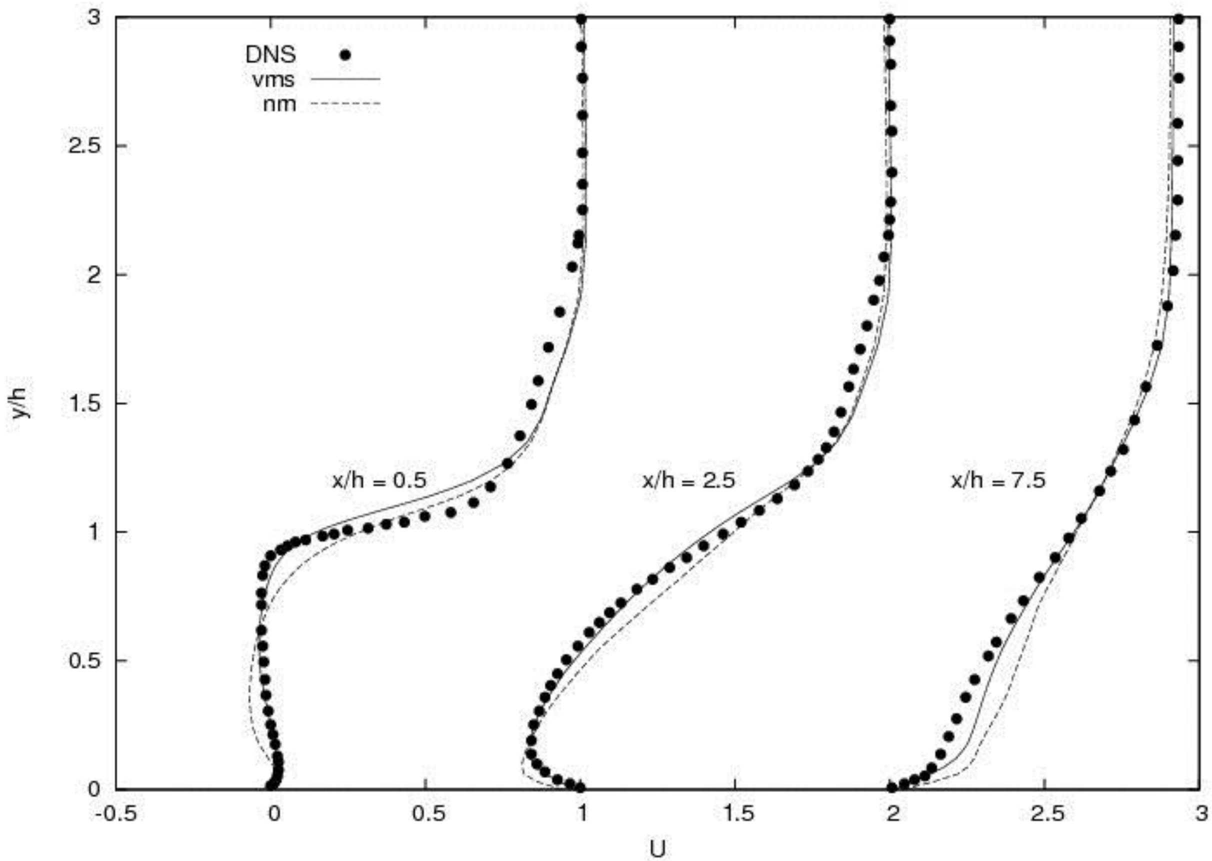

- Grid: 40000 CVs.
- VMS (box filter of lengtł 2) and symmetry-preserving discretizatioı (no modelling).
- DNS results by Le, Moin and Kim (J. Fluid Mech., 330:349-374, 1997); staggered grid of 68x192x64 CVs (aprox. 9.5 M CVs).

DNS/LES/RGM –Flow Around a Circular Cylinder (Re_D=3900)

- DNS results: power spectra of the streamwise and cross velocity fluctuations at the centerline and x/D=3
- Domain: [-4D, 20D],[-8D,8D],[0,L_z=πD]. Grid:10 M CVs (64 planes in periodic direction). Similar results with L_z=2πD and 20 M CVs (128 planes).

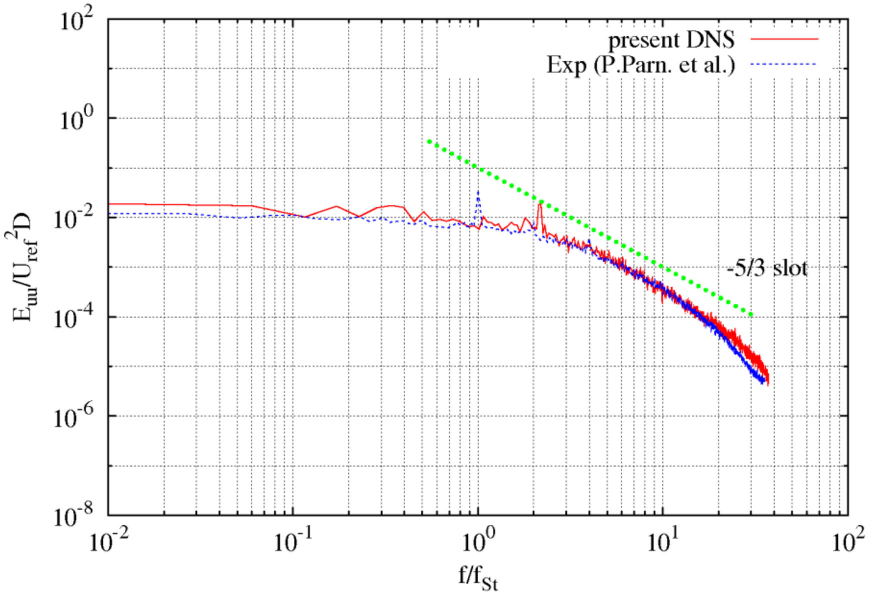

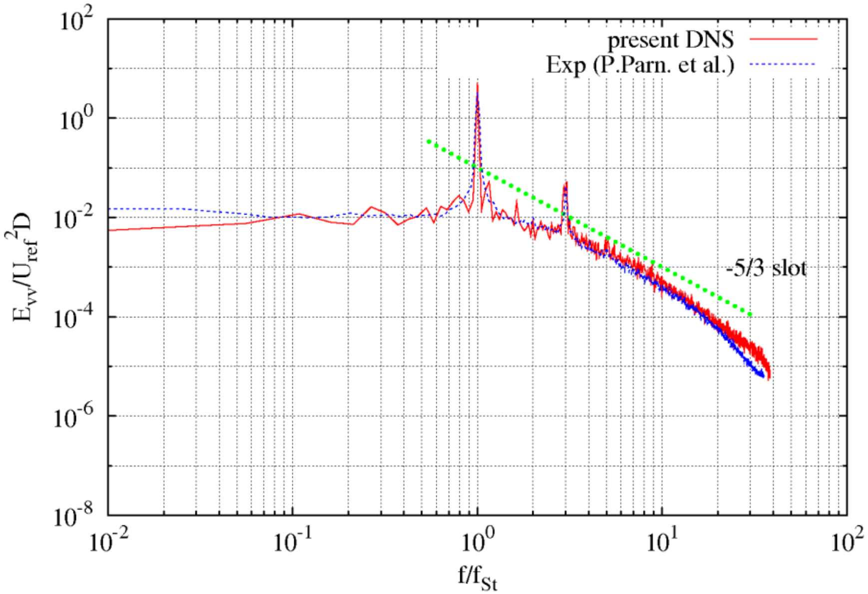

- Experimental data by Parnadeau et al (Physics of Fluids 20, 085101, 2008).

DNS/LES/RGM –Flow Around a Circular Cylinder (Re_D=3900)

- Average streamwise velocity at three locations in the wake (x/D=1.06, 1.54 and 2.02). Reynolds stresses in the streamwise direction at 1.54.
- C_4 symmetry-preserving regularization modelling with a mesh of 0.35 MCVs (vs. DNS results using 10 M CVs)

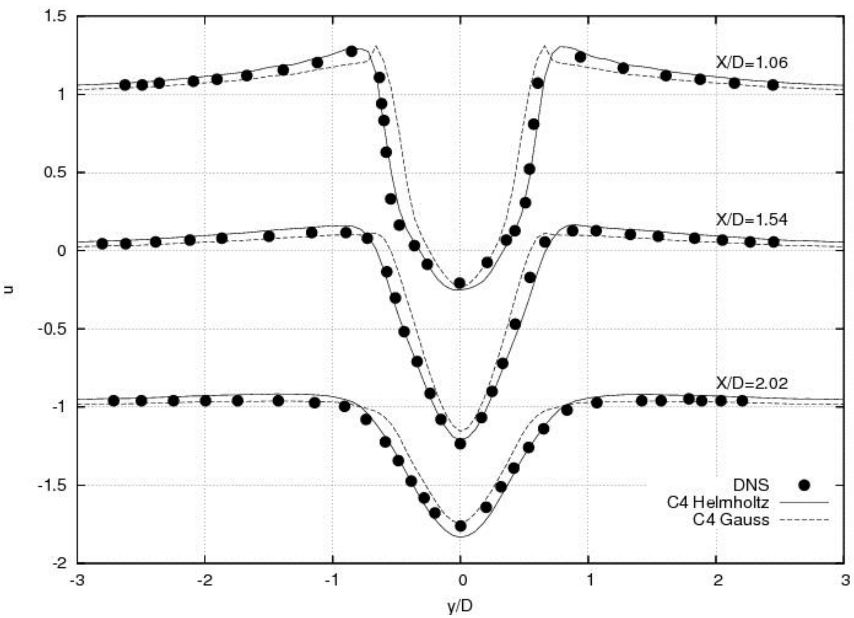

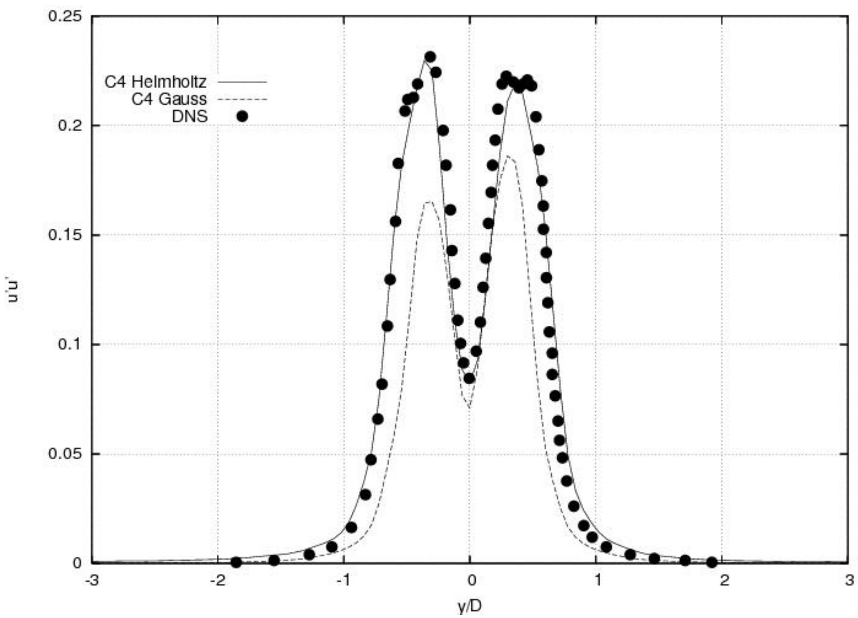

- Two filters: Gaussian vs. Helmholtz.

DNS/LES/RGM –Flow around a sphere (Re_D=3700)

- Instantaneous vortical structures in the wake of the sphere and streamwise velocity at three locations in the wake.
- Mesh II: 3.2 M CVs (64 planes in θ-direction). Mesh III: 5.5 M CVs (96 planes)

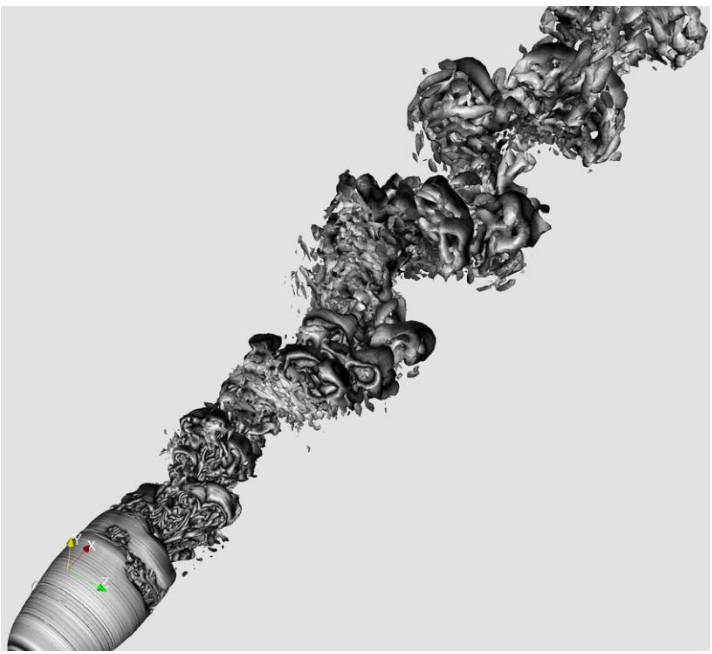

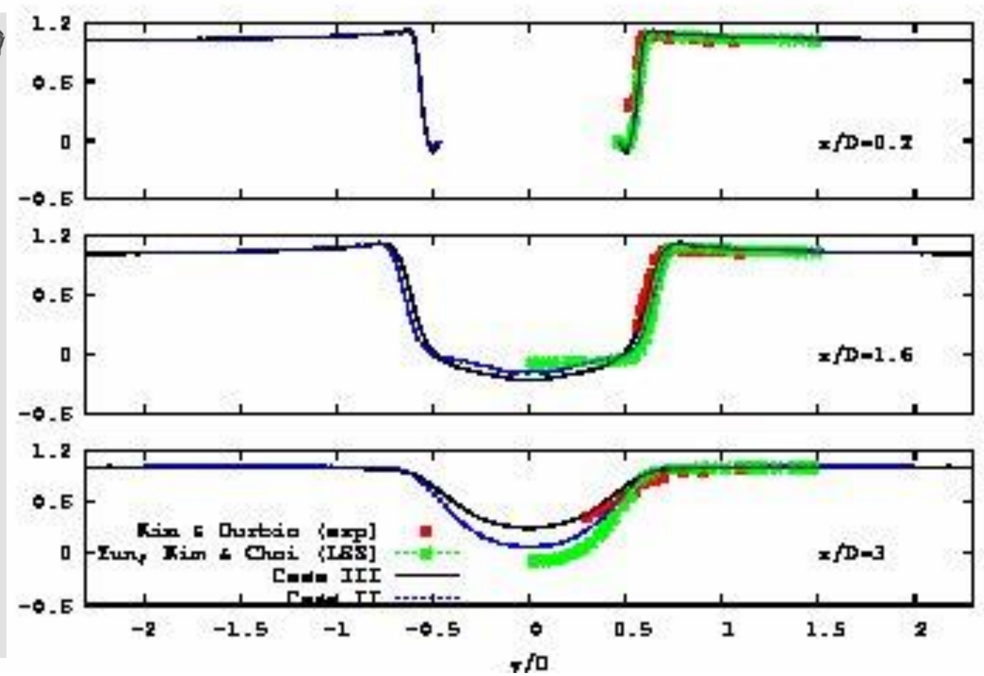

Experimental data by Kim & Durbin (Phy. Fluids 31:3260-3265, 1988); LES results by Yun et al (Phy. Fluids 18, 2006).

DNS/LES –Impinging Plane Jet Flow (Re_B=20000, H/B=4)

- Mean velocity and rms normal velocity fluctuation in x-direction and at three different locations.
- C_4 symmetry-preserving regularization modelling. Two different grids are used: 11.136 CVs (m1), and 94.080 CVs. (m2)

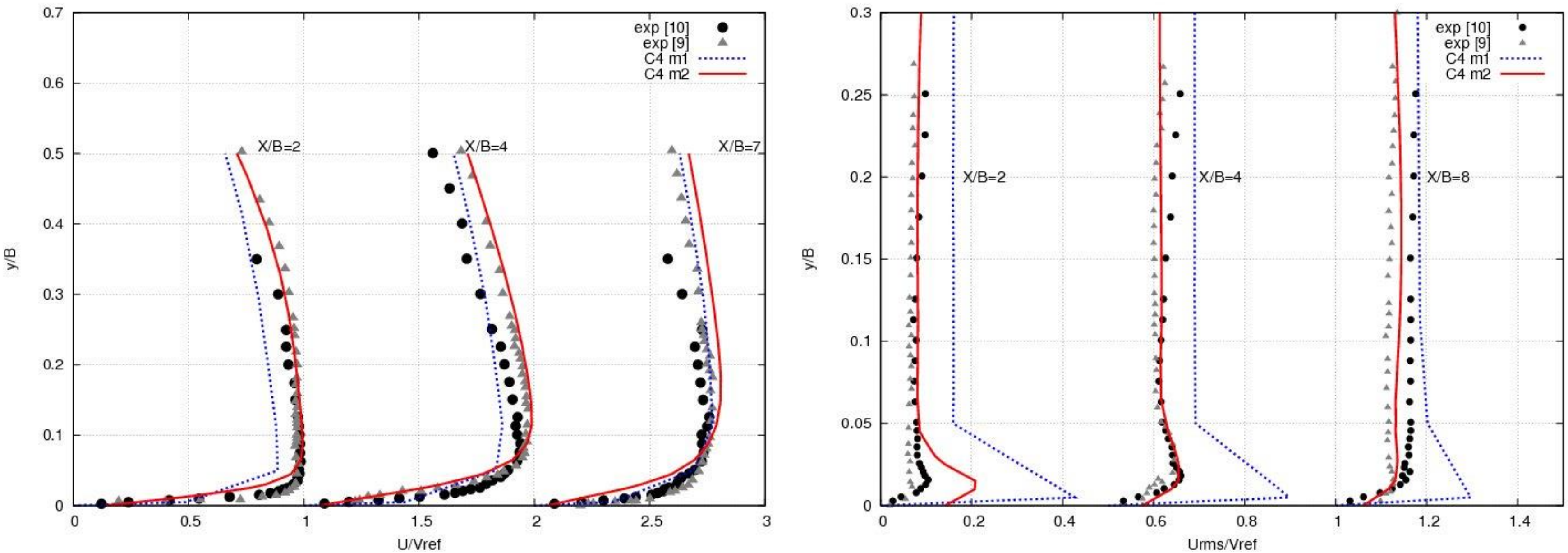

- Experimental data by Ashforth-Frost et al. (Exp. Therm. Fluid Sc., 14(1):60-67, 1997) and Zhe and Modi (J.Fluids Eng. 123(1):112-120, 2001)

DNS/LES/RGM –Industrial Applications – Flat plate solar collector

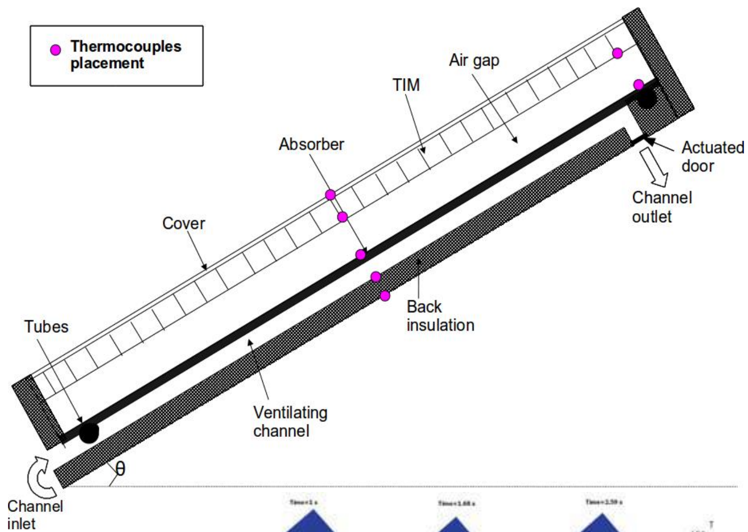

- Advanced flat plate solar collector (FPSC)
- Honeycomb transparent insulation materials (TIM)
- Overheating protection system (ventilation channel inserted at the rear top of the collector to protect the collector from stagnation conditions.)
- High thermal performance
- Industrial applications for temperature range 80 to 120 °C

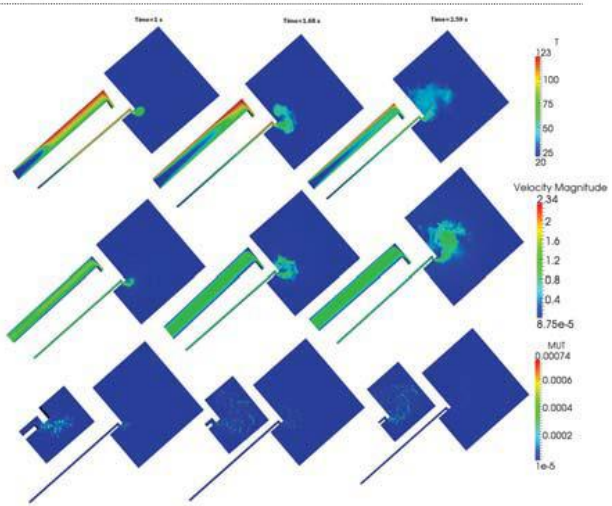

CFD simulation of the air channel (overheating protection system)

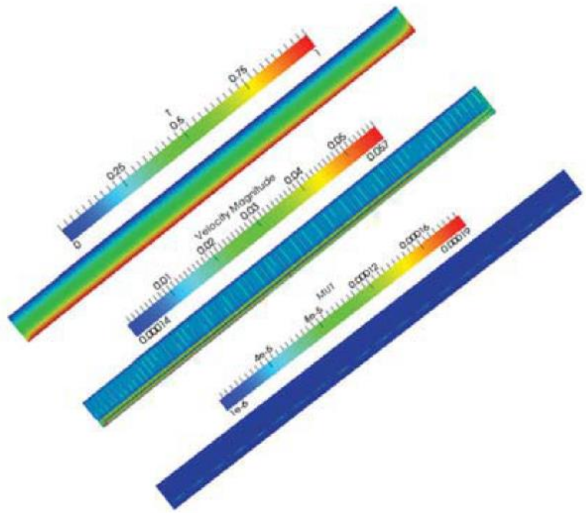

CFD simulation of the air gap +TIM

DNS/LES/RGM –Industrial Applications – Wind Energy

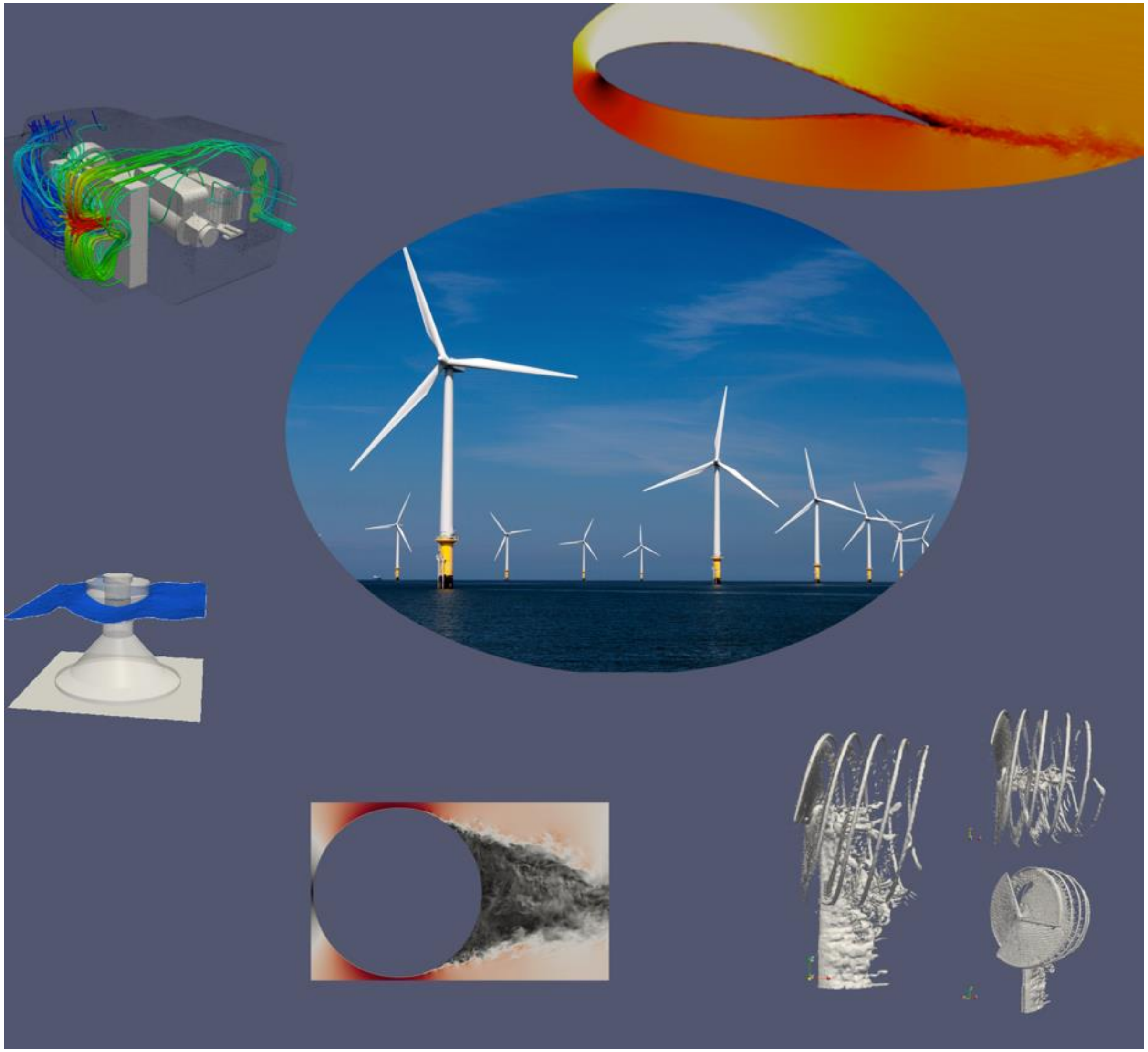

- All the elements of the wind farm are modelled using the common interface of NEST framework
- Not all the physics can be joined in a single simulation
- More computational power is needed to achieve our vision
- The most critical parts of the system can be simulated with advanced models taking to account interactions with the rest of the elements by means of reduced models

DNS/LES/RGM –NASA Common Research Model

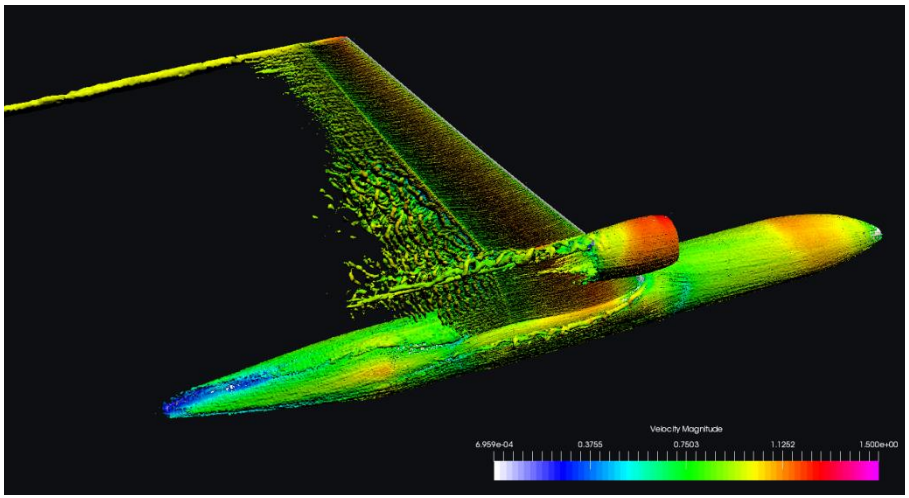

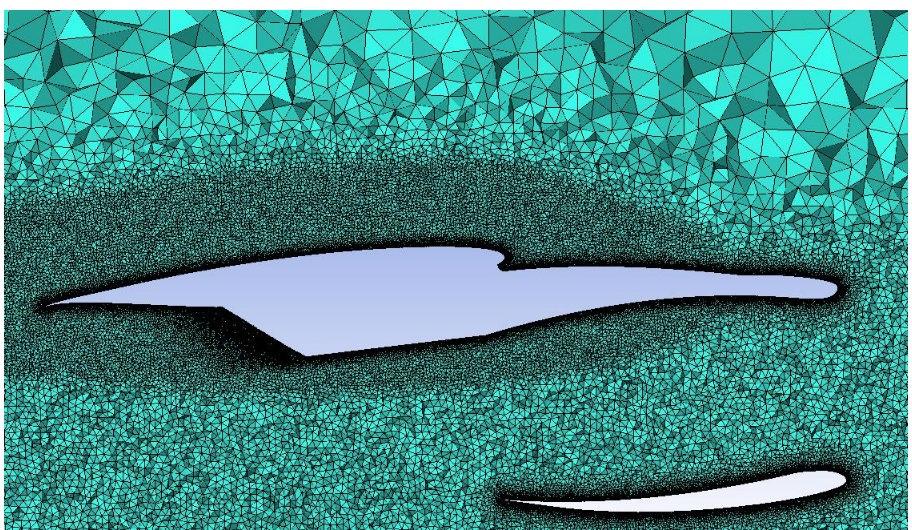

- Shear stress wall models applied on Wall Modeled LES (WLES) in the external aerodynamics
- Low dissipation schemes for convective terms
- Dynamic Smagorinsky model as SGS closure

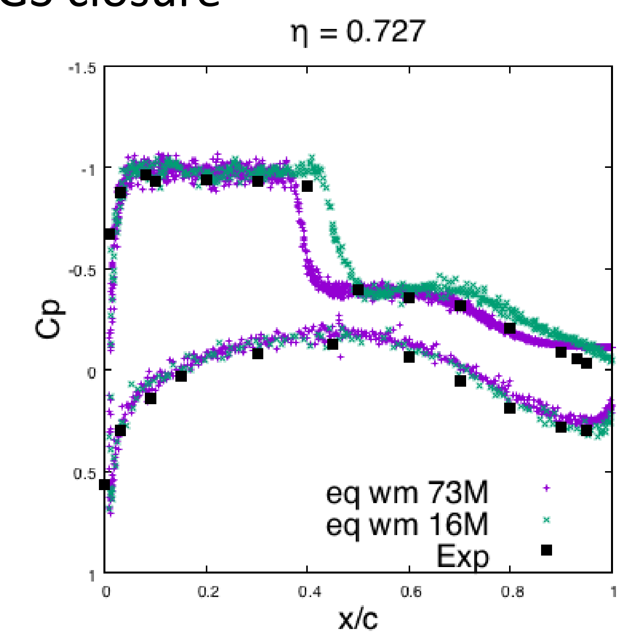

Part C. Solar Thermal Electricity (STE/CSP)

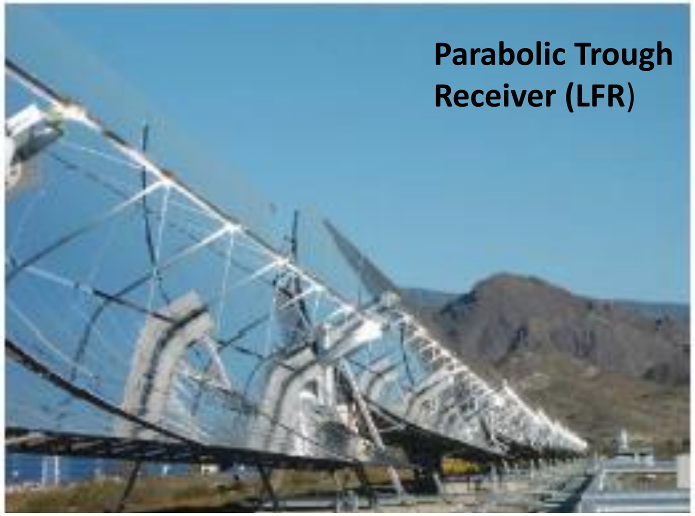

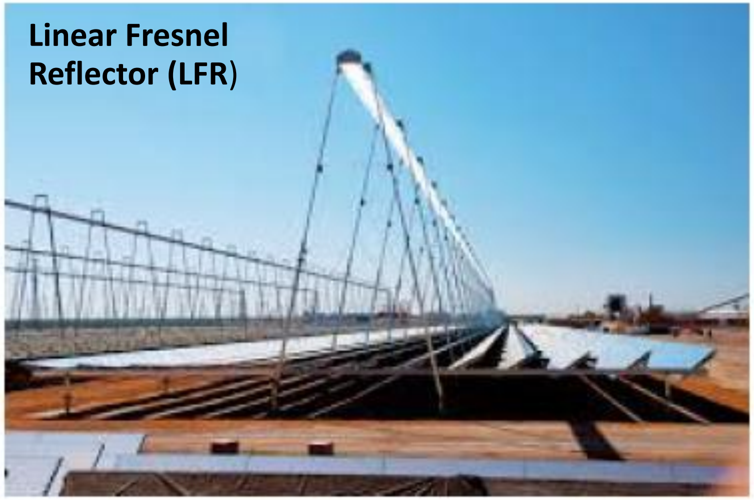

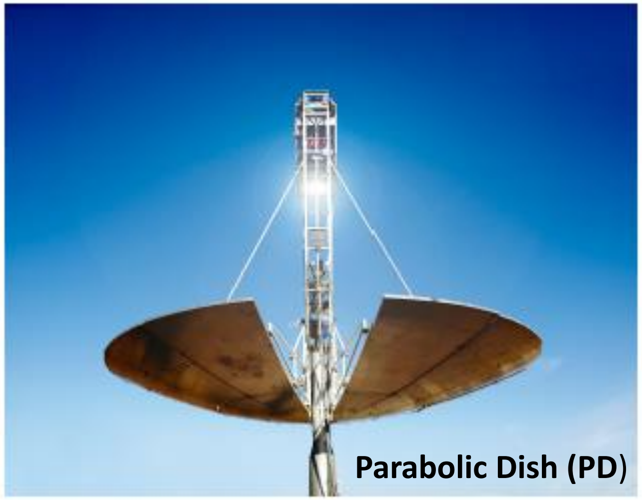

Concentrated Solar Power (CSP). Some important topics

- **Electricity** is produced using solar energy.
  - Rankine cycle. Vapour, directly produced in the solar field or indirectly through a HTF (Heat Transfer Fluid), is expanded in a steam turbine. In some designs, TES can be easily implemented.
  - Brayton cycle. Air is heated in the receiver.
- A region is **suitable for CSP** if it receives a sunlight radiation (Direct Normal Irradiance, DNI) larger than 2000 kWh/m2/yr (south of Spain: 2200 kWh/m2/yr, some locations in the south of the USA: 2700 kWh/m2/yr)
- **Installed power** CSP plants (Dec 2015): 5000 MW
- **Thermal energy storage** (TES) allows better dispatchability (ability of the plant to increase/decrease the output on demand) and higher power capacity factor (related to the fraction of time that a plant operates at full power).

Main CSP technologies

- **Central solar receiver/tower**(CR): i) a field of heliostats concentrate radiation on a central receiver; ii) dual-axis sun tracking , *C=300-1000*; iii) can operate at higher temperatures than PTC (565ºC vs. 390ºC); iv) deployed capacities: 20 MW (Gemasolar, Sevilla, Spain, MS), 110 MW (Antofagasta, Chile, MS), 392 MW (Ivanpah, California Mojave Desert, USA, 3 solar towers, DSG), etc.

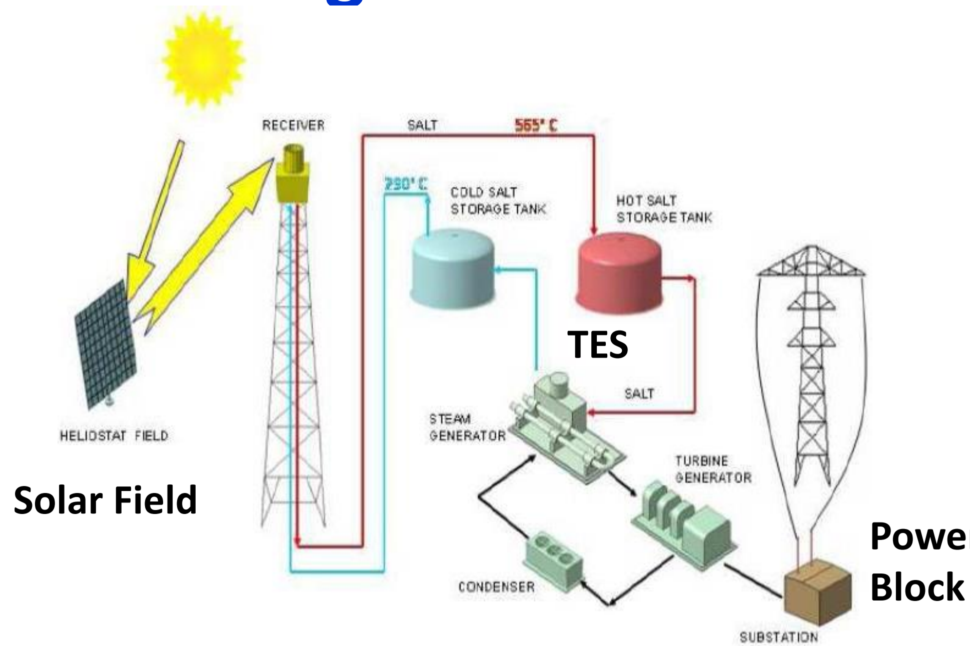

- **Parabolic trough collector** (PTC): i) parabolic mirrors concentrate radiation on a linear receiver, *C=30-100*; ii) one-axis sun tracking (east-west); iii) deployed capacities: 50 MW (Andasol, Spain), 280 MW (Solana, Arizona, USA), etc.

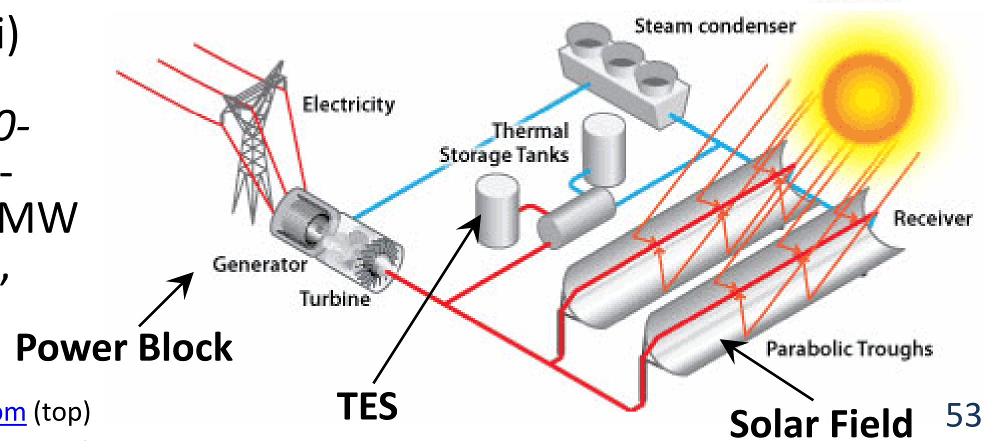

Figures from http://mcensustainableenergy.pbworks.com (top)
http://stem-works.com/ (bottom)

Other CSP technologies

- **Linear Fresnel reflector** (LFR):
  i) similar to PTC but using almost at mirrors, , *C≈30*; ii) mirrors rotate on its longitudinal axis to track the sun which is reflected on the receiver; iii) deployed capacities: 30MW (Puerto Errado 2, Calasparra, Spain), 125MW (Rajasthan, India) both using direct steam generation (DSG).

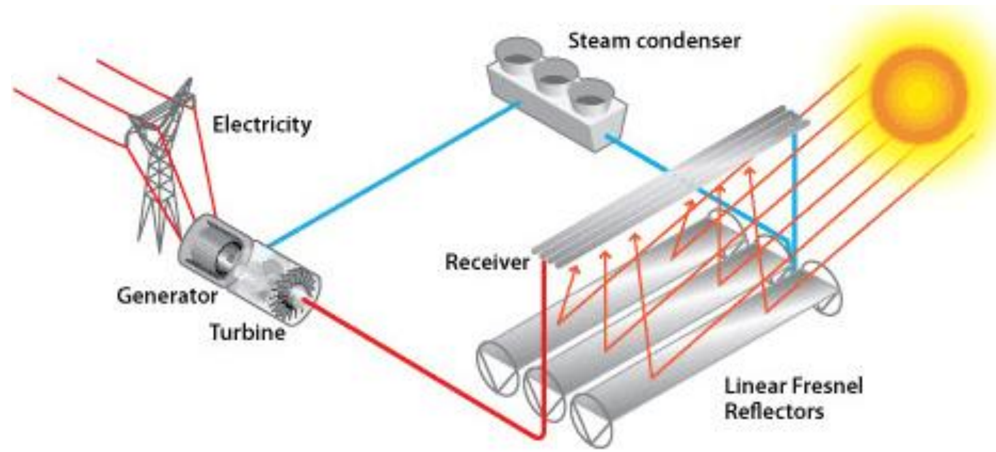

- **Parabolic dish/Stirling dish** (PD):
  i) sunlight is concentrated at the focal point (very high concentration ratios, *C≈3000*); ii) high temperatures are produced (800ºC) on the Stirling machine located at the focal point; iii) the Stirling machine drives an alternator to generate electricity; iv) very high solar-to electricity efficiency (about 30%) and highly scalable system.

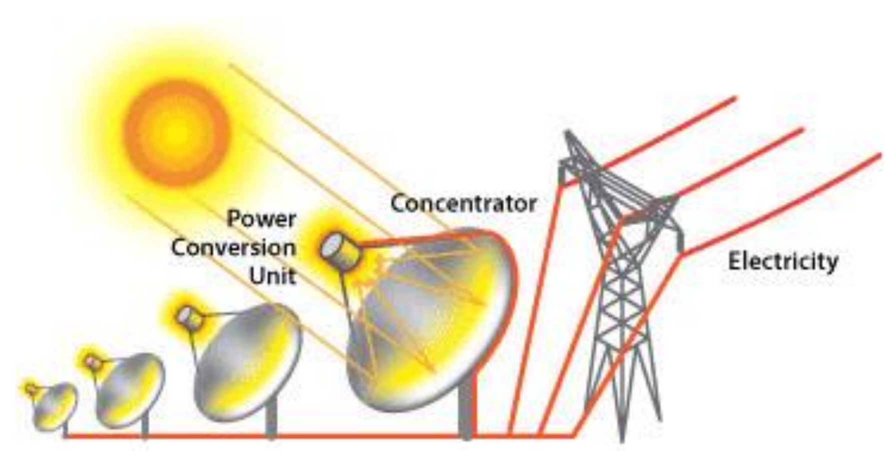

Figures from http://stem-works.com/

Central receivers (CR) and thermal energy storage (TES). Advanced multiphysic and multiscale modeling using object-oriented software and HPC platforms

Gemasolar Central Tower CSP plant

CR. Multiphysic and multiscale phenomena

- Transient conduction heat transfer at the solid elements of the receiver (tubes)
- Two-phase flow (DSG) or liquid flow (e.g. molten salts) inside the tubes of the receiver (external or cavity receiver)
- Solar radiation from the field of heliostats
- Radiative heat transfer between the surfaces of the receiver.
- Convective heat transfer between the tubes and the air surrounding them
- Thermal stresses on the tubes (fatigue) and corrosion

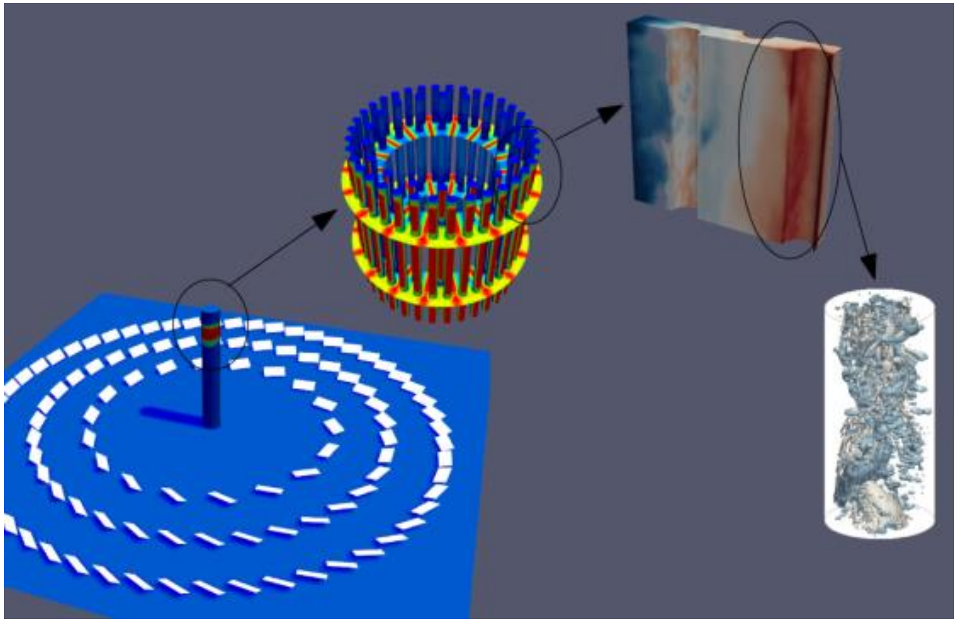

CR. Interaction between the different physical models

- Specific and independent libraries are created/used for each phy-sical phenomena
- Libraries and objects are linked through the multiphysics system library (NEST platform)
- NEST is a parallel and object-oriented platform in C++

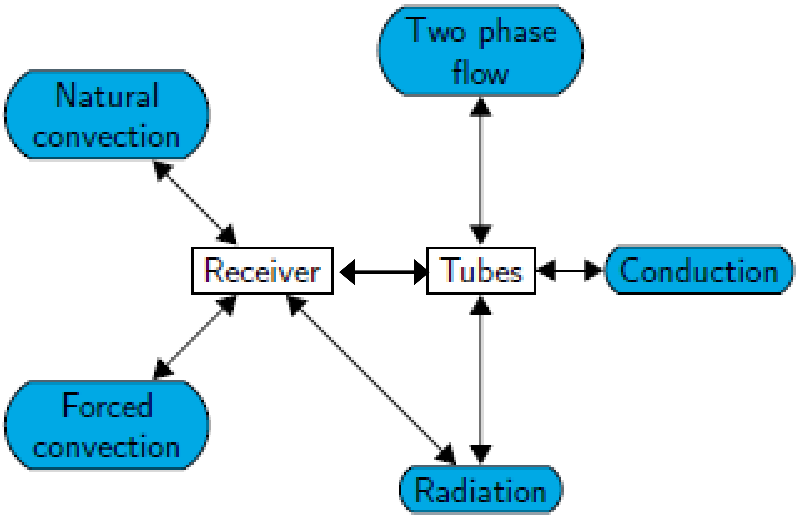

- Specific and independent libraries are created/used for each physical phenomena → modularity; different teams working t.
- Each element of a given system can be solved using a different parallelism paradigm

CR. Transient conduction heat transfer

- The conduction model is linked to all the other models through BC (insulation at the backside; solar radiation from heliostats; Infrared radiation; natural/forced convection heat transfer between the receiver and the air surroinding it; forced convection inside the tubes of the receiver)

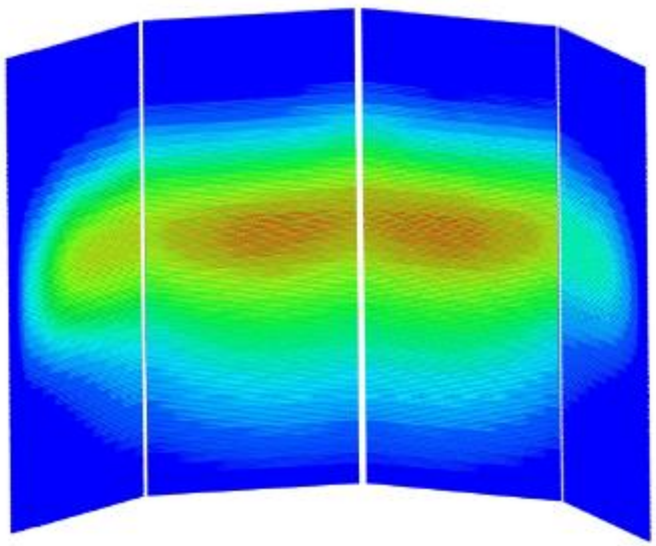

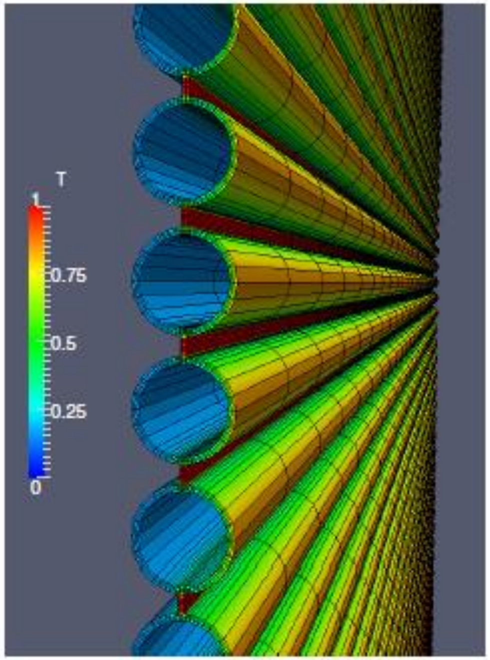

Dimensionless distribution of temperature on a receiver formed by tubes with fins between them

CR. Flow inside the tubes

- Liquid (e.g. molten salt) or two-phase flows (if DSG) in ducts could be solved using unsteady 1D models (e.g. quasi-homogeneous formulation for two-phase flow with critical heat flux models)

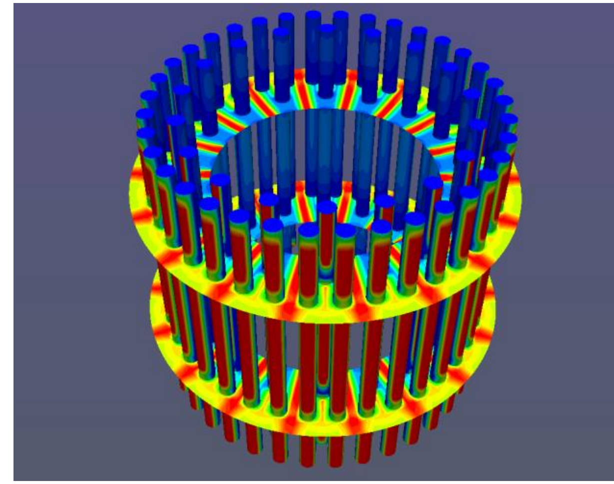

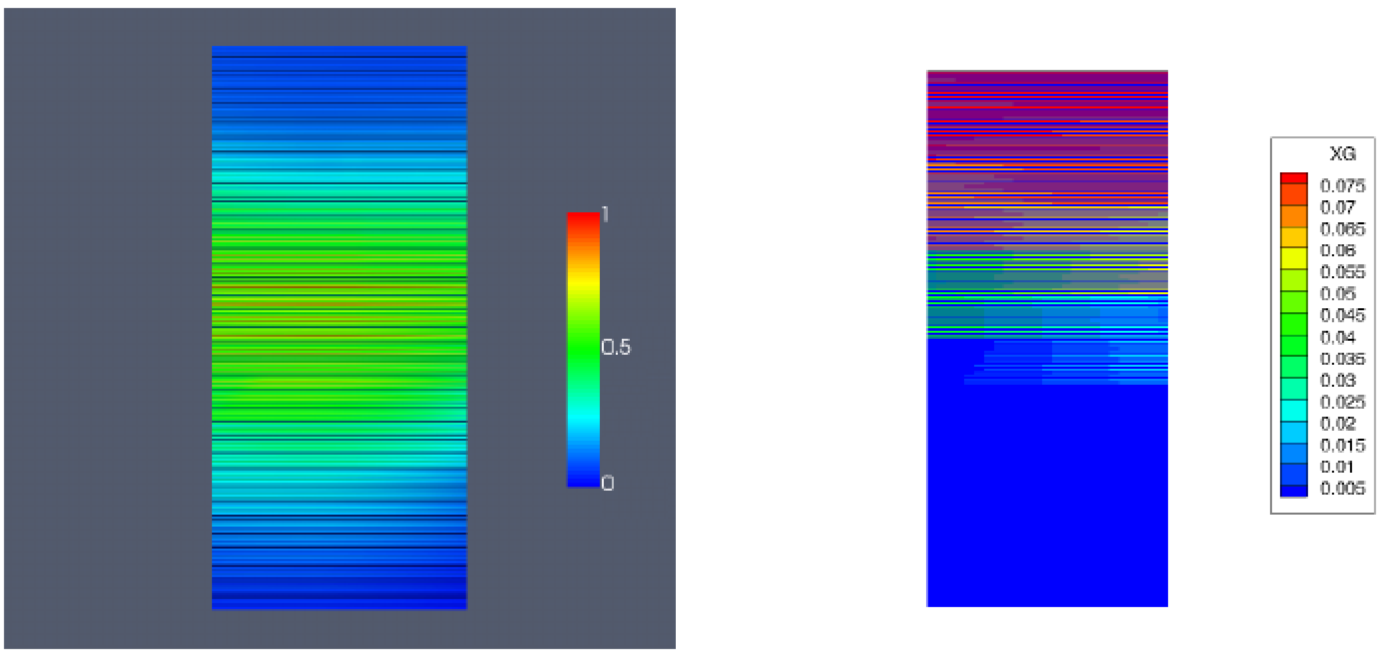

Dimensionless distribution of temperature and steam quality in a receiver panel (DSG)

CR. Radiation heat transfer overview

- Monte Carlo ray tracing method (MCRT)
- A large number of solar rays are shot from all surface elements, according to the amount of energy they emit
- When a ray hits a surface element, it may be absorbed, transmitted, reflected specularly, or reflected diffusely, according to ray wavelength and local properties
- When a ray is absorbed/emitted, the energy at the surface element is increa-sed/decreased by the energy of the ray
- Obstacles (heliostats themselves, tower, etc.
- Computationally expensive tool but efficient parallelization (each ray is independent of the others)

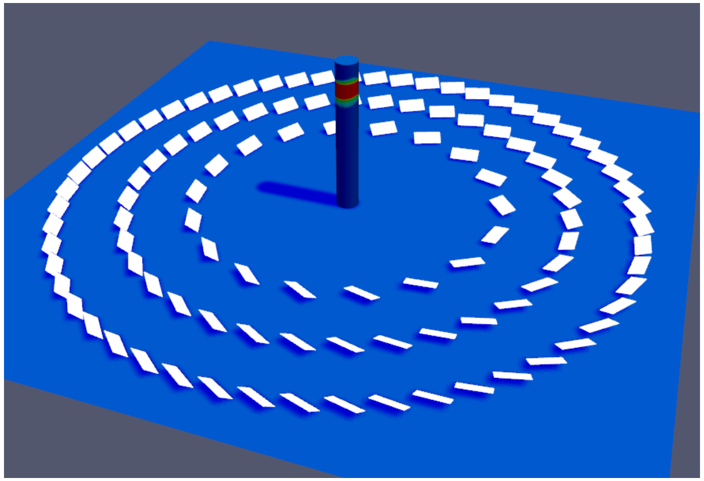

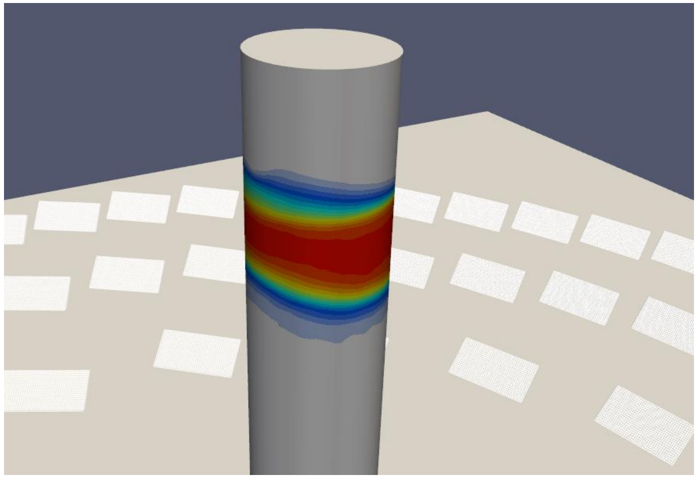

CR. Calculation of F_{ij}^{s} (with ray tracing method)

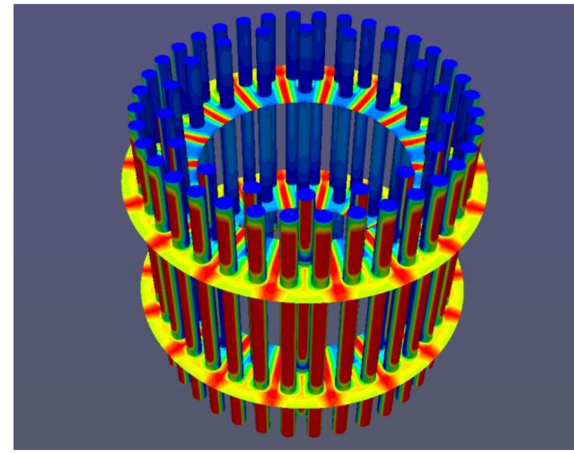

- Radiosity method (faster than MCRT)
- A number of samples is shoot from every surface and the history of each path is followed
- The sample shown contributes to $F_{\text{ab}}{}^{s}, F_{\text{ac}}{}^{s}$ and $F_{\text{ad}}{}^{s}$.
- On every reflection the energy of the sample is diminished by a factor ρ^{s} (of the reflecting surface)
- A sample is discarded when its energy falls below a minimum
- $F_{\text{ij}}{}^{s}$ is the sum of all contributions of samples shot from i that end or get reflected at j

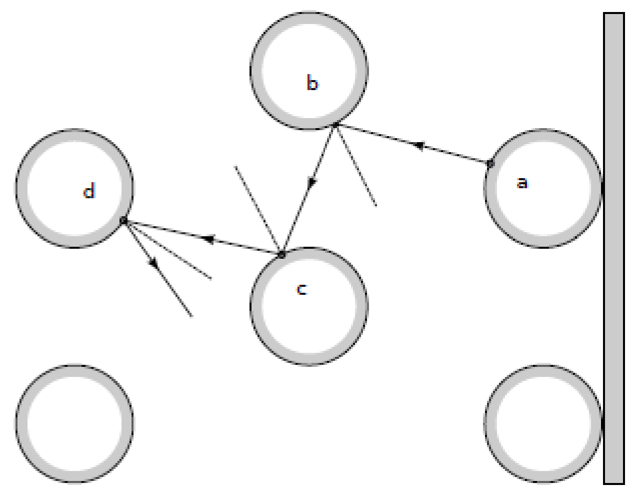

CR. External mixed convection

- Variable properties (non-Boussinesq approach).
- Small recirculation at the top corner of the cavity
- Cold fluid entrainment from the bottom of the cavity.
- There is no transition point between laminar and turbulent regime.
- Impinging phenomena near the top of the cavity.

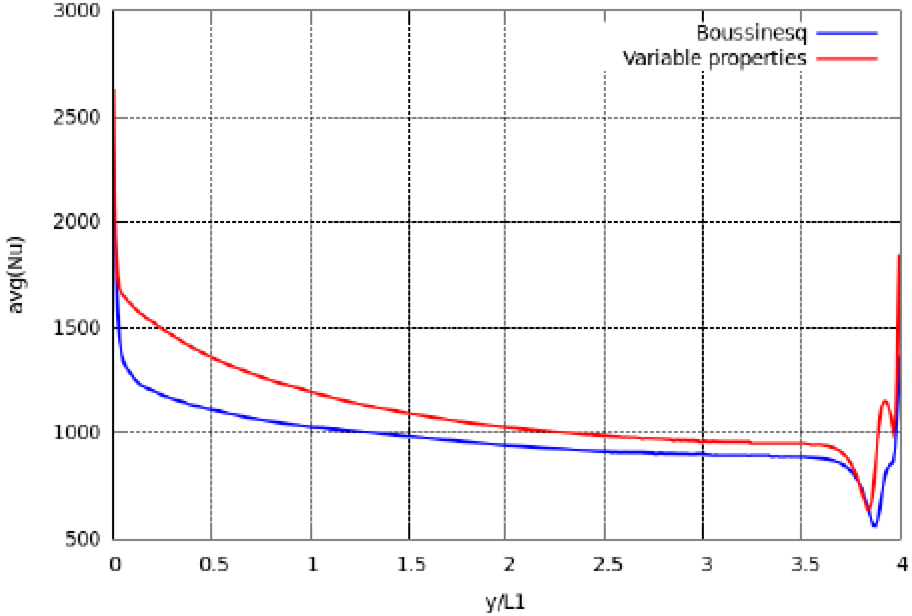

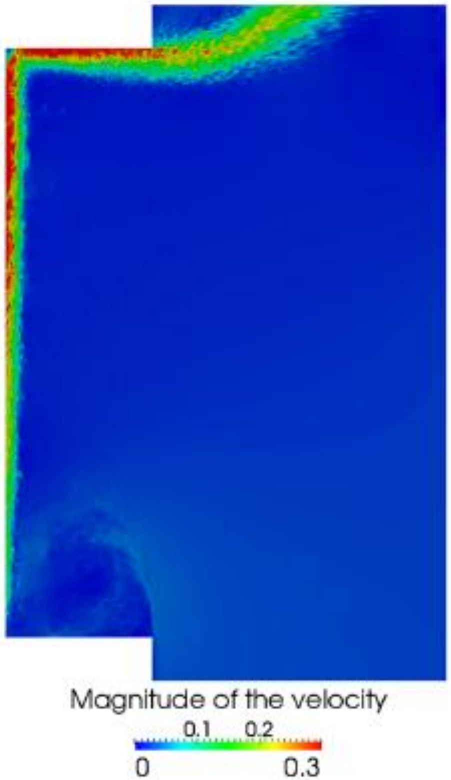

Instantaneous magnitude of the velocity and averaged Nusselt. (aspect ratio H2/L1=4, Ra = 10^{12}, Pr = 0:71.

CR. Wind effect

- Instantaneous magnitude of the velocity and Nusselt number

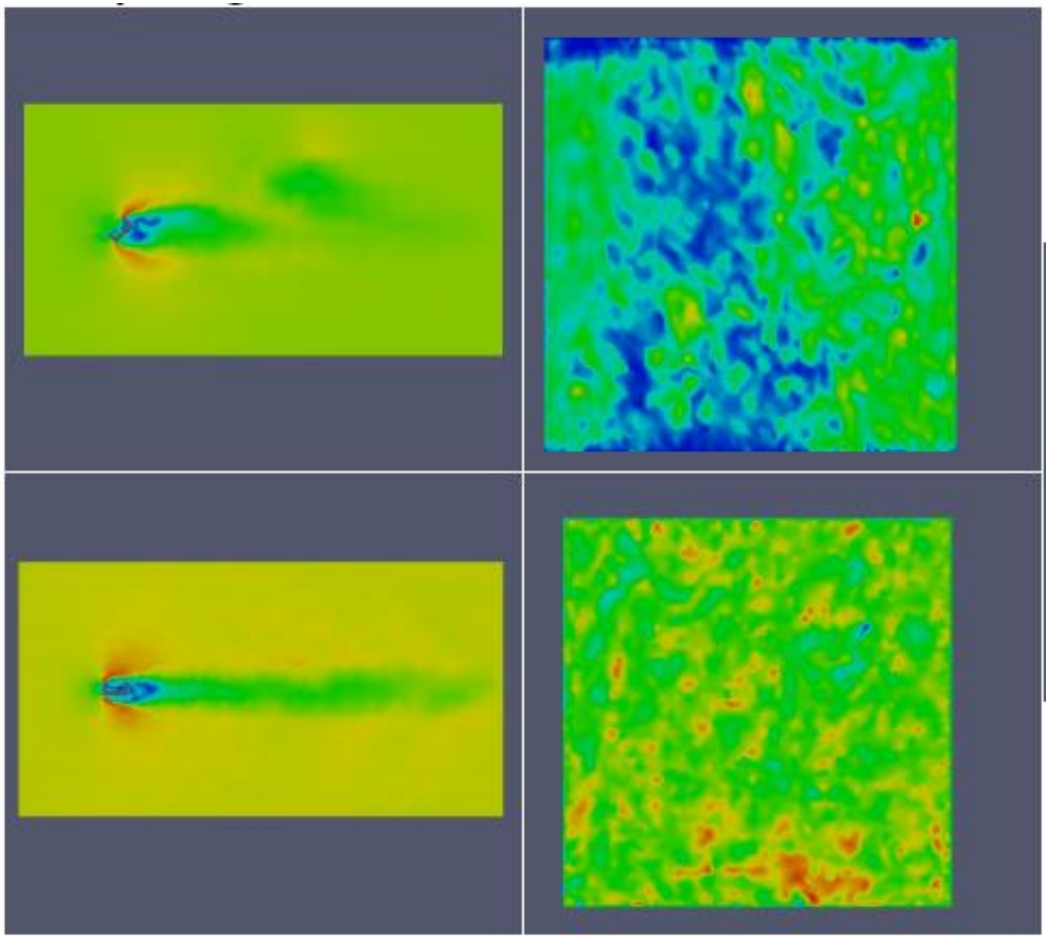

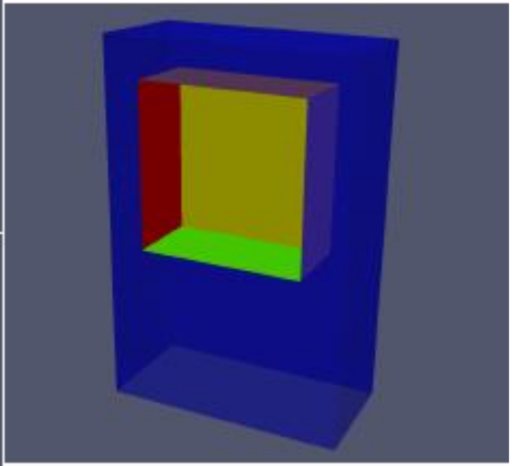

Parabolic Trough Solar Collector

New optical model

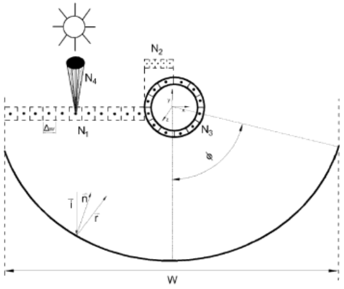

- ✓ Finite Volume methodology
- ✓ Modified Ray Tracing method

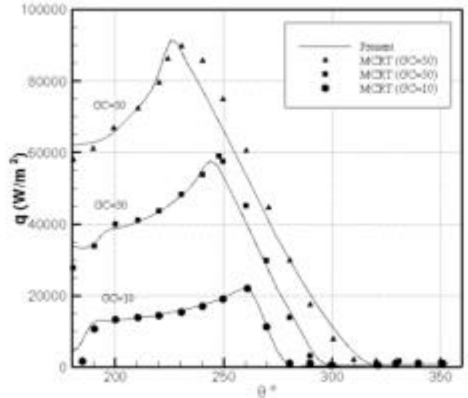

Non-uniform solar flux distribution around the receiver

Detailed unsteady and 3D thermal and fluid dynamic model of the receiver. Valid. exp. data.

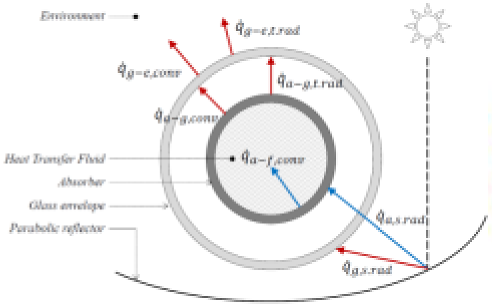

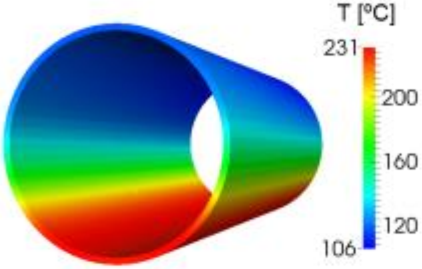

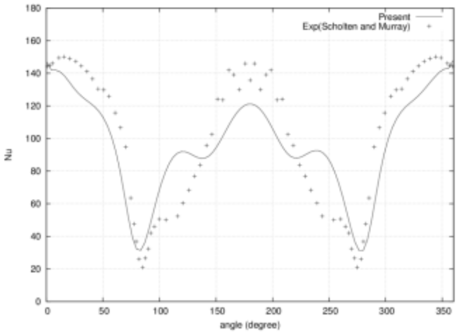

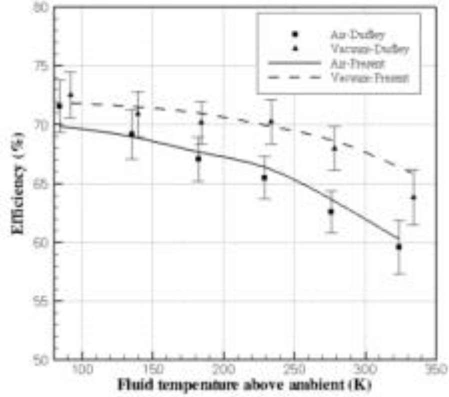

Nu vs. θ & effic. vs. Tf-Tamb

Parabolic Trough Solar Collector

Wind effect. Aerodynamic modeling

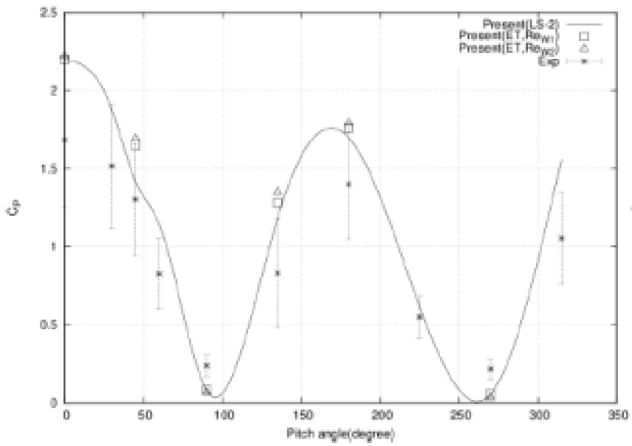

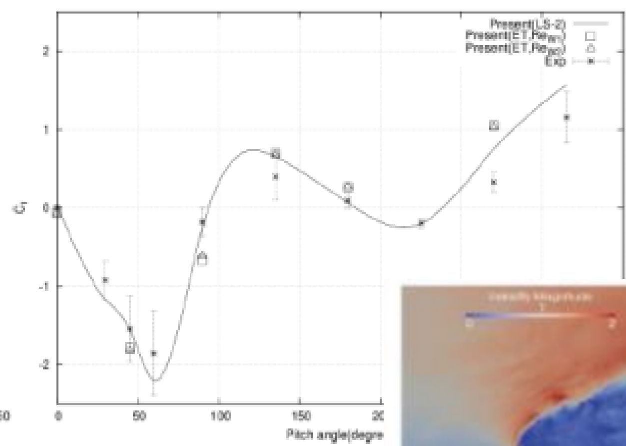

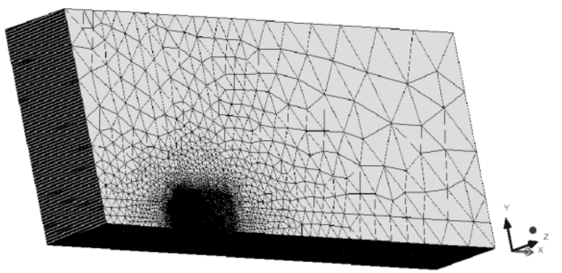

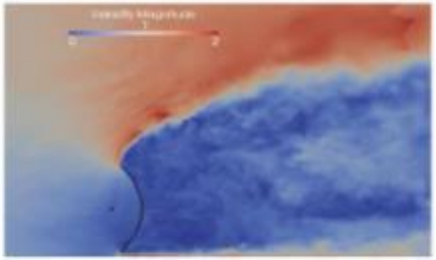

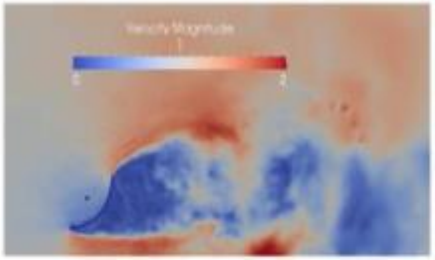

Drag and lift coefficients for different pitch angles. Good agreement with experimental results of down-scaled prototypes

Thermal stress-strain analysis. A FVM solver for thermoelastic finite deformation is used.

Thermal expansion

Thermal stresses (Von Mises [Mpa])

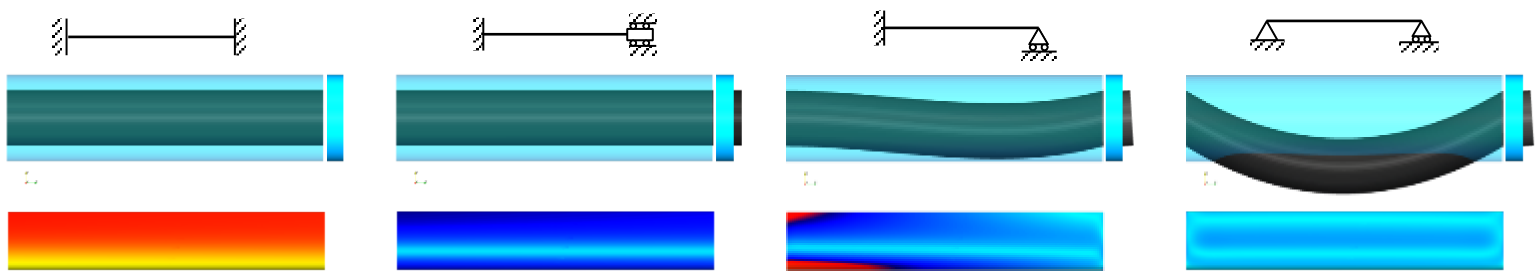

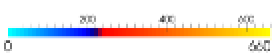

Linear Fresnel reflector

- Modular object-oriented simulation methodo-logy for the design and optimization of LFR
- Single-phase or two-phase unsteady analysis of the flow inside the tubes
- Detailed 3D conduction heat transfer in solids elements (tubes, insulation, glasses, etc.)
- Detailed analysis of the incident solar energy using Monte Carlo ray-tracing tools
- Detailed analysis of the natural convection heat transfer in the cavity of the receiver

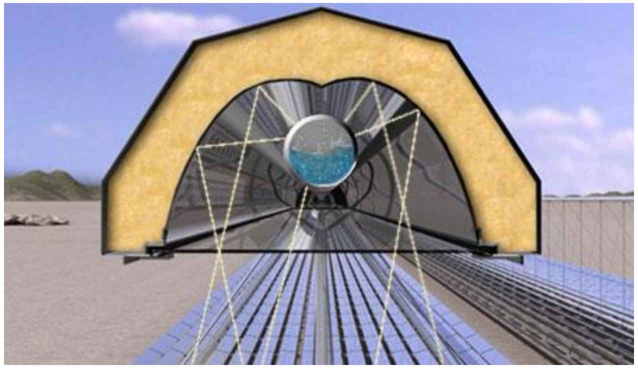

Source: Novatec

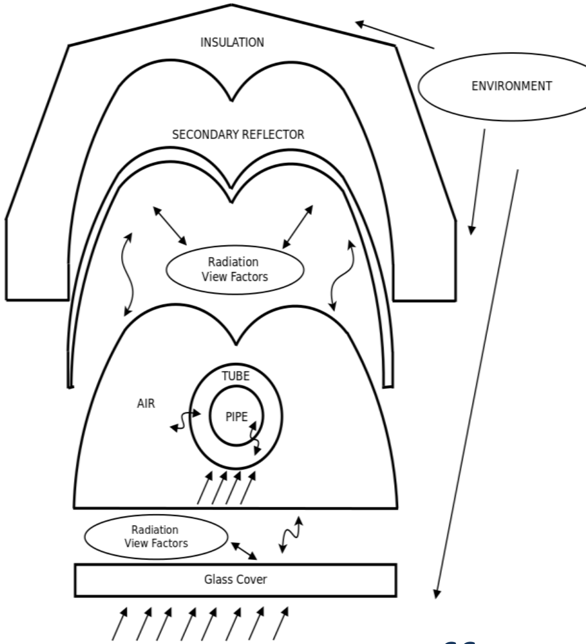

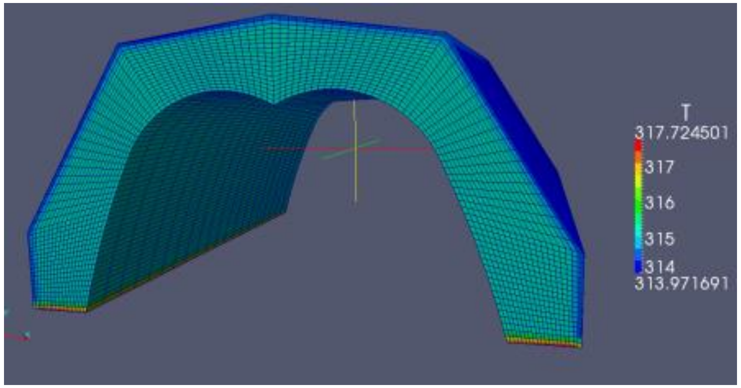

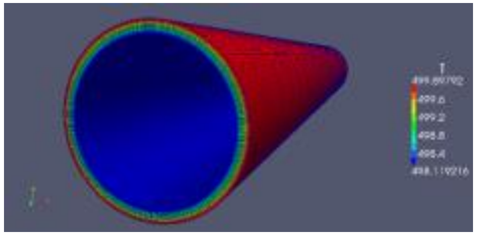

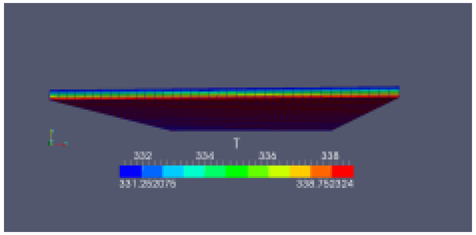

(Left) Discretization details in insulation material; (top right) Tube receiver T distribution; (bottom right) Glass cover T distribution

Linear Fresnel reflector

- CFD&HT of the air inside the cavity receiver
  - LES modeling for solving turbulent flow in the cavity
  - Heat-temperature coupling with the solids elements
  - A radiosity-irradiosity method to solve the non-participating media rad. inside the cavity
  - View factors evaluated from a ray-tracing method

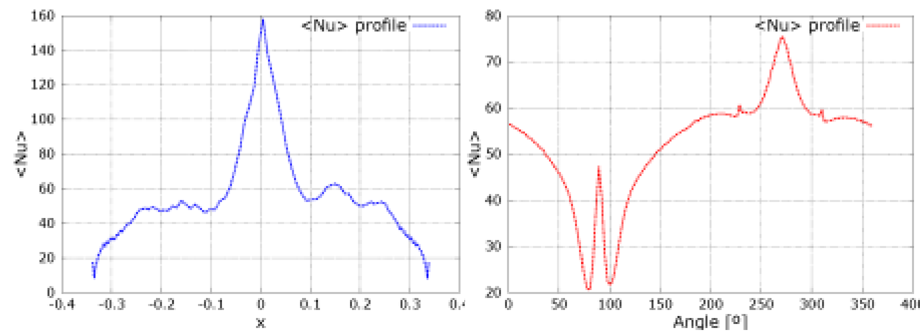

Averaged Nusselt number: insulated boundary contour (left); receiver (right)

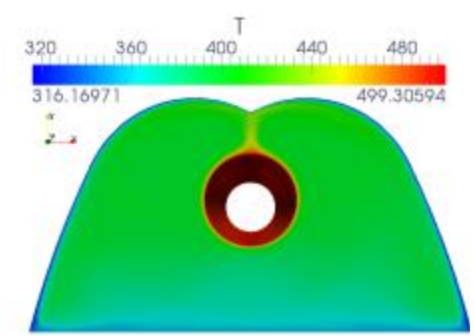

Average air temperature

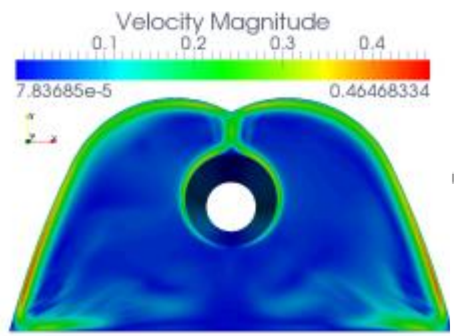

Average air flow velocity

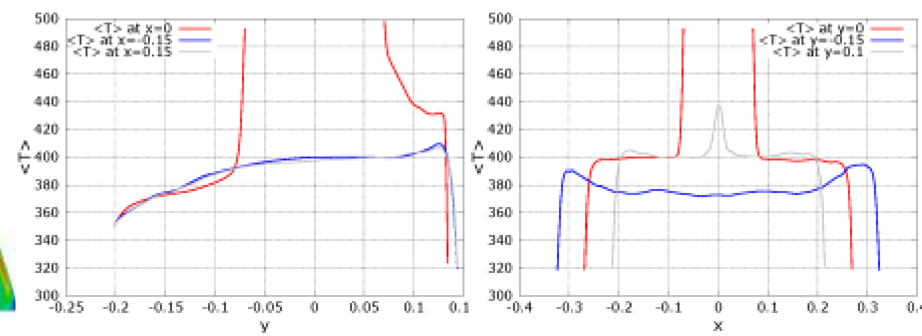

Average temperature profiles at the middle of the cavity, plane (z=0.5): vertical axis (left); horizontal axis (right)

Stirling Dish

- Forces greatly vary from one dish to the other.
- As expected, the first dish receives the larger force, it has the full effect of the high pressure bubble created by the stagnation of the incoming flow.
- Dishes 4 and 5 also experience a large force although smaller than the first dish. These two are most affected by the closing up and recirculation of the flow
- Dishes two and three exhibit a lower magnitude of force, as they are "protected" by the other dishes

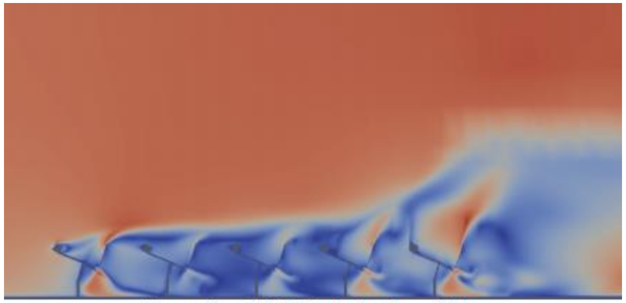

Illustration 10: Velocity in the midplane

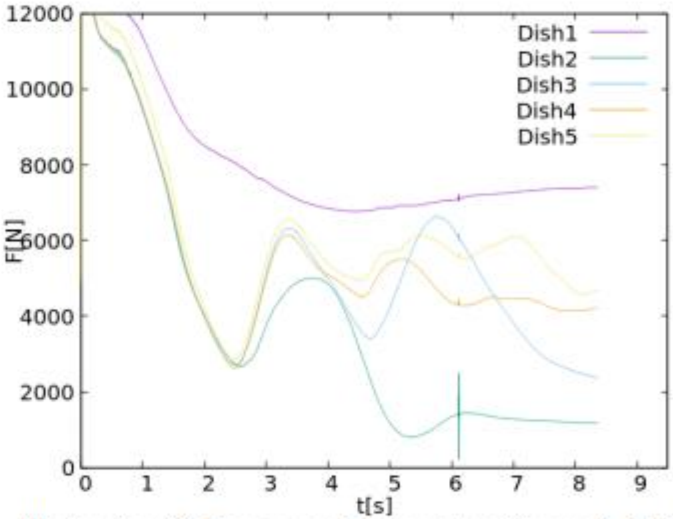

Illustration 9: Force results over time for each dish

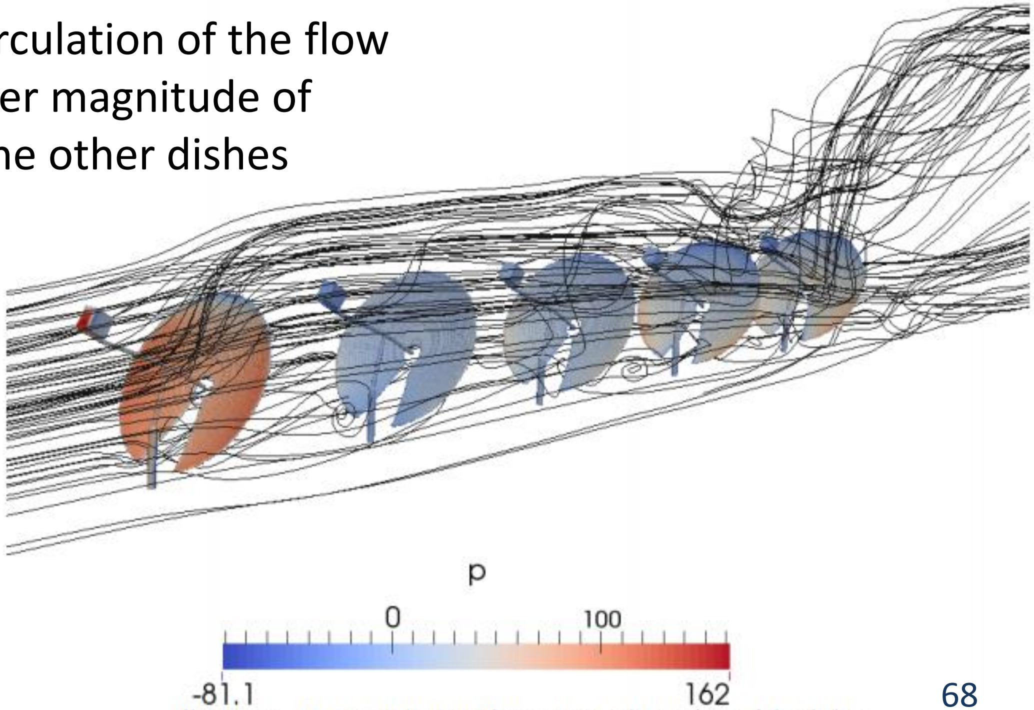

Illustration 11: Streamlines and pressure in the surface of the dishes

Two-tank TES systems

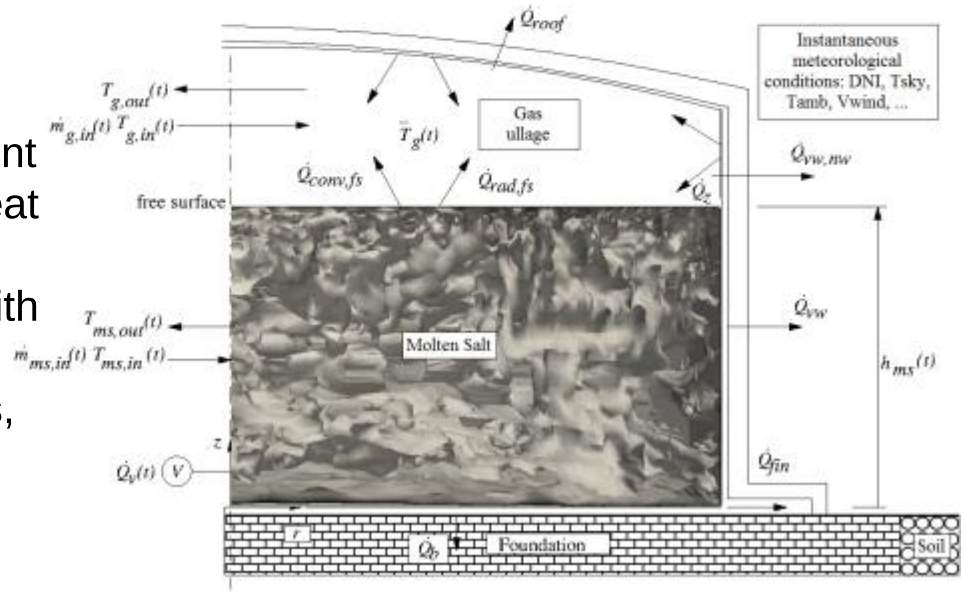

- Multi-physic nature of the system: 3D turbulent currents of the molten salt, 3D conduction heat transfer (tank walls, insulation, foundation, etc.), thermal radiation inside the tank and with the external ambient, passive cooling in the foundation, mechanical and thermal stresses, unsteady behaviour, etc.

  STEScode: specifically developed for designing purposes

- Multi-scale phenomena: advanced CFD analysis using LES methods

  Instantaneous streamlines show the movement of the salt inside the "cold" tank.

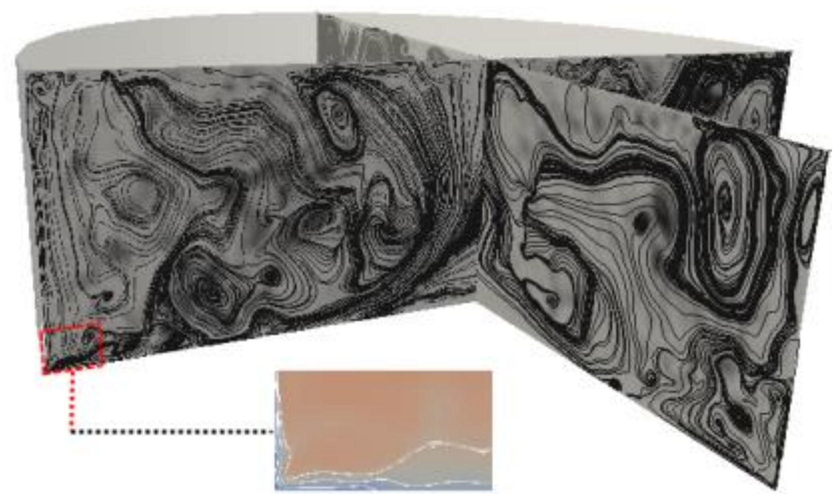

- Design aspects:

  Thermal losses control; optimization of the storage (cost reduction); how to scale up

Single-tank TES system

- Different thermocline-like systems tested: pure thermocline, single-PCM, cascade-PCM
- A new concept has been proposed: the **multilayered solid-PCM** (see figure on the right).
- Thermal and fluid dynamics linked to thermo-mechanical (thermo-elastic) analysis; advanced CFD modelling through porous media and solid-fluid interaction.
- Advanced code for design purposes: **LTEScode**.

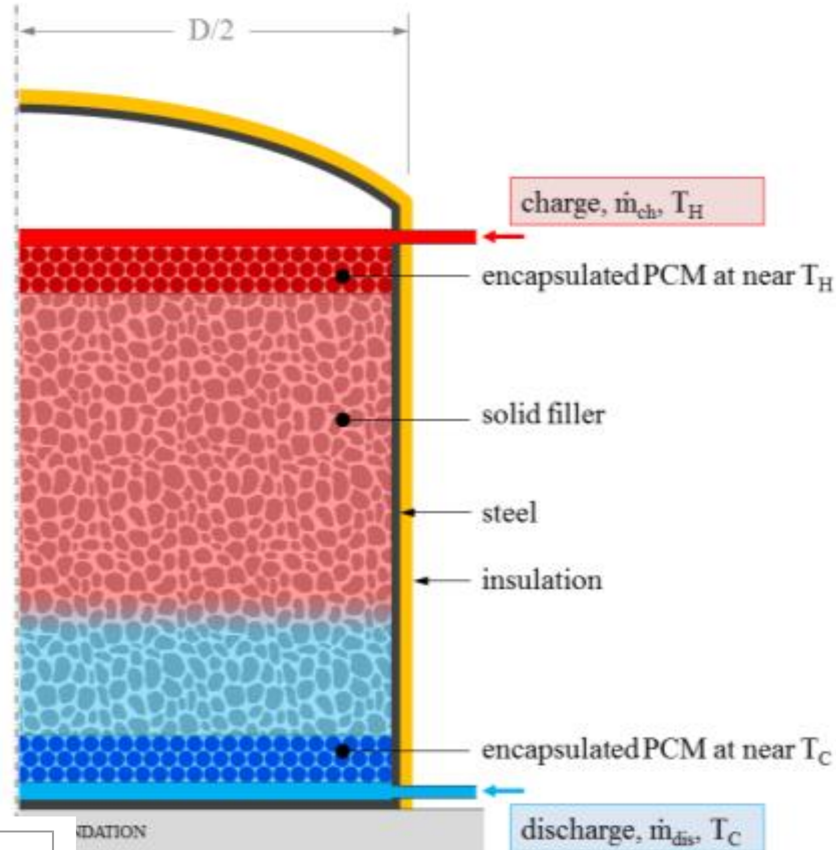

Multilayered solid-PCM

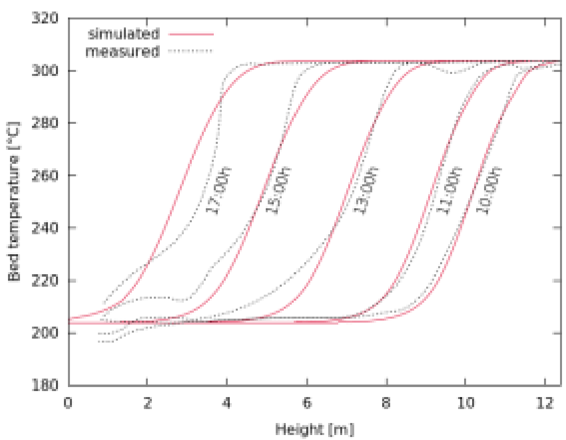

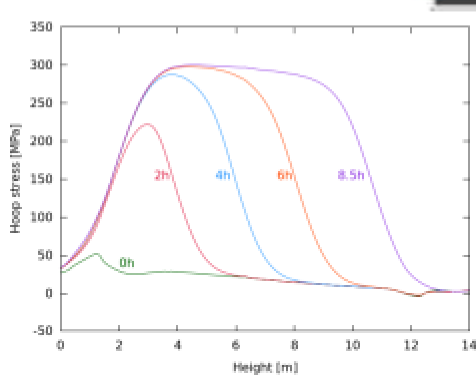

Temperature and hoop stresses distribution in a thermocline tank

D. Final comments

- Our experience: basic and applied studies are carried out simultaneously
  - Progress in the basic field increases the capacity on the applied and technology transfer field.
  - Challenges in the applied/TT fields motivate progress in the basic/fundamental lines

- Computational methods bring new possibilities in the prediction/analysis of thermal and fluid phenomena. Important issues are: physics, mathematical formulation, discretization of the equations, solvers and parallelism (HPC), V&V.

- Experimentation: physics, mathematical description, validation of computational models.

- The analysis/design/optimization of thermal systems and equipment (e.g. CSP plants components) needs:
  - Simulation of multi-physic/multi-scale problems and processes
  - Development of modular and object-oriented computation tools

CAMPUS MARE NOSTRUM 37 38

Centre Tecnològic de Transferència de Calor
UNIVERSITAT POLITÈCNICA DE CATALUNYA

Muchas gracias por su atención!

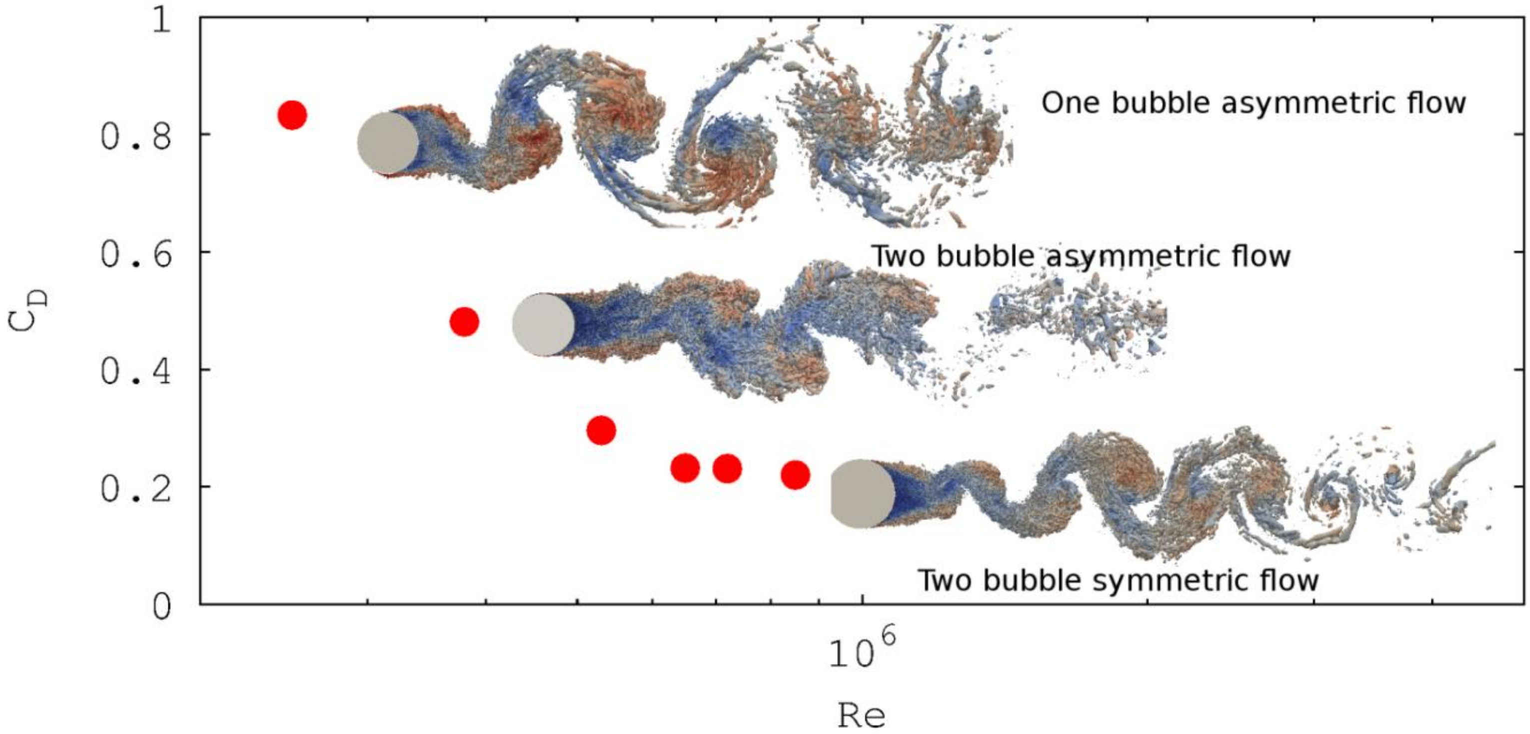

Carlos D. Perez-Segarra, CTTC (UPC), Tf. 937398192, segarra@cttc.upc.edu